Agricultural Water Management 269 (2022) 107666

Contents lists available at ScienceDirect

Agricultural Water Management

journal homepage: www.elsevier.com/locate/agwat

Development of RZ-SHAW for simulating plastic mulch effects on soil water, soil temperature, and surface energy balance in a maize field

Xiaosheng Chu [a,b], Gerald N. Flerchinger [c], Liwang Ma [d], Quanxiao Fang [e], Robert W. Malone [f], Qiang Yu [g,h,i], Jianqiang He [a], Naijiang Wang [a,b], Hao Feng [b,g,j,k,*], Yufeng Zou [b]

[a] College of Water Resources and Architectural Engineering, Northwest A&F University, Yangling 712100, Shaanxi, China
[b] Institute of Water Saving Agriculture in Arid Areas of China, Northwest A&F University, Yangling 712100, Shaanxi, China
[c] USDA-ARS, Northwest Watershed Research Center, Boise, ID 83712, USA
[d] USDA-ARS, Rangeland Resources and Systems Research Unit, Fort Collins, CO 80526, USA
[e] Qingdao Agricultural University, Qingdao 266109, China
[f] USDA-ARS, National Laboratory for Agriculture and the Environment, Ames, IA 50011, USA
[g] State Key Laboratory of Soil Erosion and Dryland Farming on the Loess Plateau, Institute of Soil and Water Conservation, Northwest A&F University, Yangling 712100, Shaanxi, China
[h] School of Life Sciences, University of Technology Sydney, Sydney 2007, NSW, Australia
[i] College of Resources and Environment, University of Chinese Academy of Sciences, Beijing 100049, China
[j] Institute of Soil and Water Conservation, Northwest A&F University, Yangling 712100, China
[k] Institute of Soil and Water Conservation, Chinese Academy of Sciences and Ministry of Water Resources, Yangling 712100, Shaanxi, China

ARTICLE INFO

Handling Editor - Dr R Thompson

Keywords:
Plastic mulch
RZ-SHAW
Energy balance
Soil water content
Soil temperature

ABSTRACT

A shortcoming of the RZ-SHAW model (A hybrid version of Root Zone Water Quality Model and The Simultaneous Heat and Water Model) is that it cannot simulate the plastic mulching technology which is widely used in arid areas. Our objectives in this study were to develop RZ-SHAW to include a new plastic module, and to evaluate the model's performance over three years of maize (*Zea mays* L.) production in China. A new plastic module was added to compute changes in the shortwave and longwave radiation transfer, turbulent heat and vapor transfer from the surface, and the energy and water balances in the system associated with a plastic mulch layer. The modified RZ-SHAW model can adequately simulate soil water ($0.017\ cm^3\ cm^{-3} \leq RMSE \leq 0.030\ cm^3\ cm^{-3}$) and capture the evaporation reduction and transpiration increase under plastic mulch. The model overestimated the increased soil temperatures under plastic mulch (2.3 ℃ over the 100-cm profile) compared to the measured data (1.4 ℃). Overall, the revised RZ-SHAW model adequately simulated soil water and heat exchange under plastic mulch conditions. The modified RZ-SHAW model can be used as an effective decision tool for management optimization in plastic mulched cropland.

Software Availability

Model name: RZ-SHAW (RZWQM).
Developer: USDA Agricultural Research Service (ARS).
Year first available: 1990.
Hardware required: CPU 1 G, RAM 1 G, Disk 1 G.
Program language: Fortran.
Program size: 70 M.
Get software: https://www.ars.usda.gov/research/software/download/?softwareid= 412&modecode= 30–12–30–25.

1. Introduction

China supports 22% of the world's population with 7% of the world's arable land (Loro, 2014). Therefore, improving food production is a major goal for China. The most challenging issues occur in dryland production regions which have fewer water resources and occupy about 50% of the cultivated land. Addressing the shortage of water resources that restrict agricultural development in dryland regions is essential for ensuring food security. Many agricultural management practices to improve crop production while using less water have been tested in dryland regions over the past few decades. One of the most effective

* Corresponding author at: Institute of Soil and Water Conservation, Northwest A&F University, Yangling 712100, China.
E-mail address: nercwsi@vip.sina.com (H. Feng).

https://doi.org/10.1016/j.agwat.2022.107666
Received 5 October 2020; Received in revised form 12 April 2022; Accepted 15 April 2022
Available online 28 April 2022

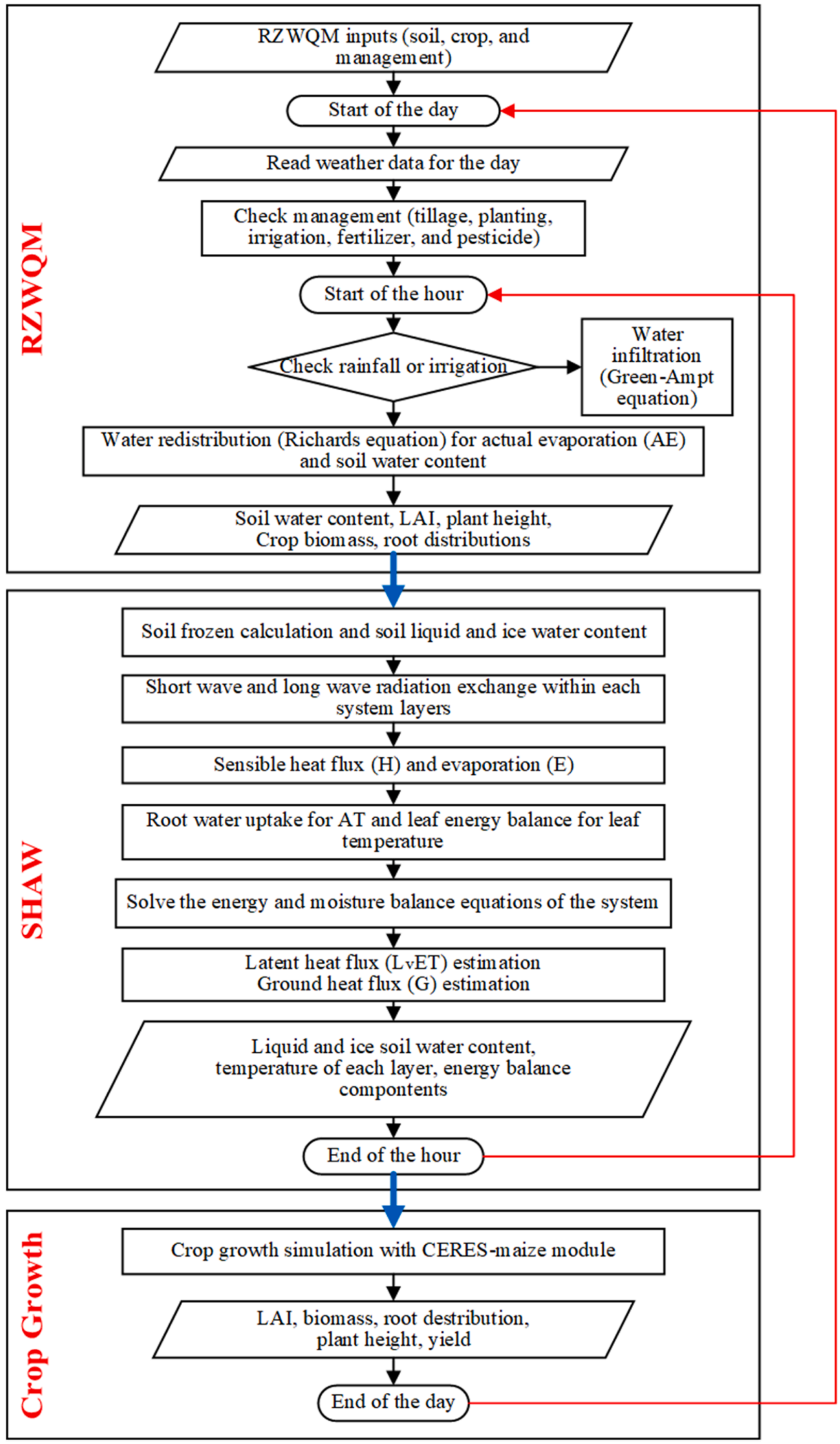

Fig. 1. Flow chart of daily and hourly execution cycles of the RZ-SHAW model.

measures is the use of plastic mulching (PM).

The use of PM has become a major management practice for rainfed farming in China (Zhang et al., 2018a), mainly due to its effects on improving moisture retention and crop yield. Zhang et al. (2018a) reported that PM increased maize yield by 4%– 245% compared with non-mulched management across the Loess Plateau in China. At the same time, PM can reduce soil evaporation (Gong et al., 2017; Li et al., 2013b) and improve soil water storage and water use efficiency. Furthermore, PM increased soil temperature in the early growing seasons and improved seedling emergence (Cavero et al., 1996; Huang et al., 2008). However, many problems need to be addressed such as early maturity, increased water consumption, and crop failure (Bu et al., 2013; Li et al., 1999; Steinmetz et al., 2016).

Due to questions regarding the effects of PM, a great deal of research has been conducted to understand the mechanisms that affect the biophysical processes. Mahrer et al. (1984) established energy balance equations of a mulched soil to describe the heat exchange process in the soil-mulch-atmosphere system, which improved the prediction of soil

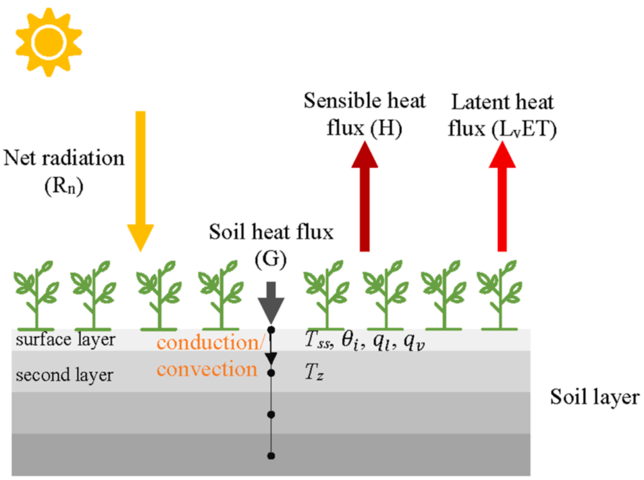

Fig. 2. Surface Energy balance in SHAW module.

moisture and temperature of a mulched soil. Chung and Horton (1987) developed a computer model which used a finite difference method to study two-dimensional coupled soil water and heat flow with a partial surface mulch. Wang and Deng (1991) analyzed the dynamics of soil energy balance components that were responsible for soil temperature increase under PM. Wu et al. (2007) built a physically-based model coupling water and heat transport in a soil-mulch-plant-atmosphere continuum. These models partly explain the effects of mulch on soil moisture, temperature, and surface energy balance in the PM system. However, these simple models usually do not consider the impact of crops or set crop parameters to fixed values during the simulation.

To quantify the effect of PM on crop growth, many researchers have used the AquaCrop model to simulate yield, biomass, and canopy cover ratios of different crops (maize, millet (*Setaria italica* L.), cotton (*Gossypium spp.*), sweet pepper (*Capsicum annuum* L.)) with PM (Cosic et al., 2017; Guo et al., 2018; Ran et al., 2017; Tan et al., 2018). However, the AquaCrop model does not consider the impact of PM on soil temperature which an important factor affecting crop growth. Han et al. (2014) modified the temperature module of the DNDC (Denitrification-Decomposition) model to analyze how soil moisture, soil temperature, and corn yield were influenced by PM. Liang et al. (2017) improved the soil water and heat modules of WHCNS (Soil Water Heat Carbon Nitrogen Simulator) using the simple empirical approach of Han et al. (2014) to identify optimal management practices among different water and N treatments in GCRPS (Ground Cover Rice Production System). However, this approach was not applicable when surface soil temperature was greater than the air temperature as often occurs in dry areas (Liang et al., 2017).

Therefore, it is necessary to study the effects of PM on soil water, soil heat, and crop growth from other perspectives (such as energy balance) in a complete crop model (such as RZ-SHAW). The RZ-SHAW model was developed by coupling the RZWQM (Root Zone Water Quality Model, Ahuja et al., 2000) and the SHAW models (Simultaneous Heat and Water Model, Flerchinger and Saxton, 1989). The RZWQM model has been fully verified and applied to farmland ecosystems (Fang et al., 2014b), and can simulate soil moisture, soil temperature, and evapotranspiration of the soil-crop system (Fang et al., 2010b; Ma et al., 2012a). The SHAW model has a very comprehensive energy balance system that performs well in simulating soil moisture, soil temperature, and the energy balance of the soil-crop system (Flerchinger, 2017; Ma et al., 2012b). The coupled RZ-SHAW model brings together the advantages and capabilities of both RZWQM and SHAW, which has been successfully tested using field data (Fang et al., 2014a; Li et al., 2012; Yu et al., 2007).

The objectives of this study were to: (1) add a plastic mulch submodule to RZ-SHAW based on energy balance and water balance equations; (2) test the performance of the modified RZ-SHAW model for simulating soil temperature and water content using three years of data (2014–2016) from a maize field; and (3) explore differences between simulated evapotranspiration and surface energy fluxes between a plastic mulch and control treatment to ensure that simulations are reasonable and to gain a better understanding of the processes influencing observed soil temperature and moisture.

2. Model descriptions

2.1. Brief description of the RZ-SHAW model

In the RZ-SHAW model, the SHAW model was linked to RZWQM to simulate surface energy balance to overcome: the shortcomings of assuming surface soil temperature equal to air temperature in the original RZWQM; and the inability of SHAW to simulate crop growth (Li et al., 2012; Ma et al., 2012b; Yu et al., 2007). A simplified representation of the execution sequence for RZ-SHAW is shown in Fig. 1.

At the beginning of each day, the model reads the input daily or hourly meteorological data, and then checks all of the management practices and creates the management queue. If there is a rainfall or irrigation event, the model executes the Green-Ampt equation to calculate infiltration. Between rainfall or irrigation events, the soil water is redistributed by using the Richards equation:

$$\frac{\partial \theta}{\partial t} = \frac{\partial}{\partial z}\left[K(h,z)\frac{\partial h}{\partial z} - K(h,z)\right] - S(z,t) \qquad [1]$$

where θ is volumetric soil water content (cm^3 cm^{-3}), t is the time at an hourly time step, z is soil depth (cm, assumed positive downward), h is soil water pressure head (cm), K is unsaturated hydraulic conductivity (cm h^{-1}, a function of h and z), and S(z, t) is a sink term for root water uptake (RWU) and tile drainage rates (hr^{-1}). RWU in the sink term is from SHAW and described later. The surface boundary condition is an evaporative flux until the soil surface water potential falls below a minimum value (set at −20,000 cm), at which time a constant head condition is used:

$$-K\frac{\partial h}{\partial z} + K = E \qquad [2]$$

where E is the evaporation rate at the soil surface (cm hr^{-1}). Soil evaporation, E, from SHAW was used in this study when the surface water potential was above the minimum value. When surface water potential falls below the minimum water potential or if the E exceeds the capability of the soil to deliver water to the surface based on the Richards equation (Fang et al., 2014a), actual evaporation (AE) is limited by the RZWQM routines. The Richards (Eqn. [1]) and its boundary (Eqn. [2]) are solved by a mass-conservative, mixed form iterative finite-difference numerical solution (Celia et al., 1987, 1990).

The SHAW routines are called at the same time step (hourly or sub-hourly) as the Richards equation to simulate heat transfer and energy balance in the system. The input parameters required to run the SHAW module (soil water content, leaf area index (LAI), plant height, crop biomass, and root distributions) are provided by RZWQM. SHAW routines first determine the liquid and ice water content of the soil for temperatures less than 0 °C, and then update the matric potential and solute concentration in the soil (Fuchs et al., 1978; Li et al., 2012). The surface energy balance described in SHAW may be written as (Fig. 2):

$$R_n = H + L_vET + G \qquad [3]$$

where R_n is net all-wave radiation (W m^{-2}), H is sensible heat flux (W m^{-2}), L_vET is latent heat flux (W m^{-2}), G is soil or ground heat flux (W m^{-2}), L_v is latent heat of evaporation (J kg^{-1}), and ET is actual evapotranspiration from the exchange surface and plant canopy (kg m^{-2} s^{-1}). R_n is defined by the equation:

$$R_n = S_b + S_d - S_u + L_d - L_u \qquad [4]$$

where S_b and S_d are direct (or beam) and diffuse downward shortwave radiation incident on the surface, S_u is shortwave radiation reflected by the surface to the sky, L_d is downward longwave radiation emitted from the atmosphere, and L_u is longwave radiation emitted from the surface to the atmosphere.

Shortwave and longwave radiation exchange and amounts absorbed by each layer above the soil surface are computed according to Flerchinger (2017), Flerchinger et al. (2009), and Flerchinger and Yu (2007). Direct, and upward and downward diffuse radiation being transmitted, reflected, and absorbed are considered when calculating the energy exchange among canopy, snow, residue, or soil layers. The upward flux of diffuse shortwave radiation ($S_{u,i}$) and longwave radiation ($L_{u,i}$) above canopy layer i are determined by:

$$\begin{aligned} S_{u,i} = \ & [\tau_{d,i} + (\alpha_{l,d,i}f_{d,i,\downarrow\downarrow} + \tau_{l,d,i}f_{d,i,\downarrow\uparrow})(1-\tau_{d,i})]S_{u,i+1} \\ & +(\alpha_{l,d,i}f_{d,i,\downarrow\uparrow} + \tau_{l,d,i}f_{d,i,\downarrow\downarrow})(1-\tau_{d,i})S_{d,i} \\ & +(\alpha_{l,b,i}f_{b,i,\downarrow\uparrow} + \tau_{l,b,i}f_{b,i,\downarrow\downarrow})(1-\tau_{b,i})S_{b,i} \end{aligned} \quad [5]$$

$$\begin{aligned} L_{u,i} = \ & [\tau_{d,i} + (1-\varepsilon_c)f_{d,i,\downarrow\downarrow}(1-\tau_{d,i})]L_{u,i+1} \\ & +(1-\varepsilon_c)f_{d,i,\downarrow\uparrow}(1-\tau_{d,i})L_{d,i} \\ & +\frac{1-\tau_{d,i}}{\sum_{j=1}^{NP}(1-\tau_{d,i,j})}\sum_{j=1}^{NP}(1-\tau_{d,i,j})\varepsilon_c\sigma T_{l,i,j}^4 \end{aligned} \quad [6]$$

where $\tau_{d,i}$ is the transmissivity of canopy layer i to diffuse radiation, $\tau_{b,i}$ is the transmissivity of canopy layer i to direct (or beam) radiation, $\alpha_{l,b,i}$ and $\tau_{l,b,i}$ are the effective albedo and leaf transmittance of canopy layer i to direct radiation, $\alpha_{l,d,i}$ and $\tau_{l,d,i}$ are the effective albedo and leaf transmission to diffuse radiation within canopy layer i, $f_{b,i,\downarrow\uparrow}$ and $f_{d,i,\downarrow\uparrow}$ are the fractions of reflected direct and diffuse radiation scattered backwards (e.g., downward radiation scattered upwards), $f_{b,i,\downarrow\downarrow}$ and $f_{d,i,\downarrow\downarrow}$ are the fractions of reflected direct and diffuse radiation scattered forwards, $S_{d,i}$ and $S_{b,i}$ are downward diffuse and direct radiation entering canopy layer i, ε_c is the emissivity of the canopy elements, $\tau_{d,i,j}$ is the diffuse transmissivity for plant j and of layer i, and $T_{l,i,j}$ is the leaf temperature of plant *j* in canopy layer i. The radiation exchange equations for the crop residue layer are similar to that for the crop canopy, and a similar expression can be written for downward radiation at any layer.

After computing net radiation fluxes, the turbulent transfer coefficients for both H and ET fluxes from the surface are calculated. H is calculated from temperature gradients between the exchange surface and the atmosphere (Campbell and Norman, 1998):

$$H = -\rho_a c_a \frac{T_{c/sn/r/ss} - T_a}{r_H} \quad [7]$$

where ρ_a, c_a, and T_a are the density (kg m^{-3}), specific heat (J kg^{-1}°C^{-1}), and temperature (°C) of air at the measurement reference height, $T_{c/sn/r/ss}$ is the temperature of the canopy, snow, residue, or soil surface, and r_H is the resistance to the surface heat transfer (s m^{-1}) corrected for atmospheric stability. Actual ET used to calculate latent heat flux at each time step is calculated from vapor density gradients between the exchange surface and atmosphere (Flerchinger, 2017):

$$ET = \frac{\rho_{v,c/sn/r/ss} - \rho_{va}}{r_v} \quad [8]$$

where $\rho_{v,c/sn/r/ss}$ and ρ_{va} are vapor density (kg m^{-3}) at the exchange surface (canopy, snow, residue, or soil surface) and at the reference height, and r_v is the resistance value for vapor transfer.

The RWU needed in the Richards equation, and equal to actual transpiration (AT), is calculated by a difference in water potential between soil and plant xylem (Flerchinger and Pierson, 1991):

$$AT = RWU = \sum_{i=1}^{NS}\frac{\psi_{s,i} - \psi_x}{r_{r,i}} \quad [9]$$

where $\psi_{s,i}$ and ψ_x are water potentials (m) in layer i of the soil and the plant xylem, respectively. NS is the number of soil nodes. The resistance to water flow (m^3 s kg^{-1}) through the roots of layer i, $r_{r,i}$, is calculated by dividing total root resistance for the plant by its fraction of roots within the soil layer. Leaf temperature for each plant species within each canopy layer is calculated with a leaf energy balance equation described by (Flerchinger, 2017).

The energy balance equation for temperature distribution in the soil matrix, considering convective heat transfer by liquid and latent heat transfer by vapor for a layer of freezing soil, is given by:

$$C_s\frac{\partial T_s}{\partial t} - \rho_i L_f\frac{\partial \theta_i}{\partial t} = \frac{\partial}{\partial z}[k_s\frac{\partial T_s}{\partial z}] - \rho_l c_l\frac{\partial q_l T_s}{\partial z} - L_v(\frac{\partial q_v}{\partial z} + \frac{\partial \rho_v}{\partial t}) \quad [10]$$

where C_s and T_s are volumetric heat capacity (J kg^{-1} °C^{-1}) and temperature (°C) of the soil, ρ_i is density of ice (kg m^{-3}), θ_i is volumetric ice content (m^3 m^{-3}), k_s is soil thermal conductivity (W m^{-1} °C^{-1}), ρ_l is density of water, c_l is specific heat capacity of water (J kg^{-1} °C^{-1}), q_l is liquid water flux (m s^{-1}), q_v is water vapor flux (kg m^{-2} s^{-1}), and ρ_v is vapor density (kg m^{-3}) within the soil. The soil energy balance (Eqn. [10]) for the surface soil layer interfaces with the surface energy balance equations (Eqns. [3, 4, 7, and 8]) or the energy balance of the overlying material (canopy, snow, or residue). Surface temperature and humidity must be solved iteratively to balance all components of the surface energy balance at the soil surface (R_n, L_vET, H, and G). Energy balance equations for all layers (canopy, snow, residue and soil) throughout the profile are solved simultaneously using the Newton-Raphson method for temperature change at each node in the current time step. After a solution is obtained for a time step, the computed soil surface temperature, water and ice content can be used to calculate soil heat flux G directly from the terms in Eqn. [10] for the surface soil layer (Fig. 2):

$$\begin{aligned} G = \ & [\frac{k_{s(t)}}{\Delta z_s} + c_l q_l](T_{ss(t)} - T_{z(t)}) - \frac{\Delta z_s}{2\Delta t}[C_s(T_{ss(t)} - T_{ss(t-\Delta t)}) \\ & -\rho_i L_f(\theta_{i(t)} - \theta_{i(t-\Delta t)})] + L_v q_v \end{aligned} \quad [11]$$

where Δz_s is depth of the second soil node (m), Δt is the time step (s), $T_{ss(t)}$ is surface soil temperature at the end of the time step (°C), $T_{ss(t-\Delta t)}$ is surface soil temperature at beginning of the time step ($t - \Delta t$;°C), $T_{z(t)}$ is soil temperature of the second soil layer (°C).

The water balance equations established for the canopy and residue layers are solved simultaneously for vapor density change at each node (Flerchinger, 2017). The water balance for the soil layers of SHAW was not used in RZ-SHAW, and the mass balance of snowpack was calculated after solving the energy and water balance equations. Latent heat flux (L_vET) is the sum of the heat exchanges caused by transpiration and evaporation.

At the end of the hourly time step, SHAW outputs shortwave and longwave radiation absorbed by each layer and energy balance components (H, L_vET, G, and R_n). SHAW then provides liquid and ice water content and soil temperature to RZWQM for the next hourly step. When all hourly steps are finished for a day, the daily soil water content and soil temperature are input to the crop growth module in RZ-SHAW to update crop parameters, such as LAI, biomass, root distribution, plant height, and yield. The CERES-maize growth module was used in this study, and the theory for that module can be found in Jones et al. (2003) and Ma et al. (2006). New crop parameters are then used for the next day's loop.

2.2. Description of the plastic mulch layer submodule

The plastic mulch layer submodule was developed based on SHAW in RZ-SHAW by adding a plastic layer into the original atmosphere-canopy-

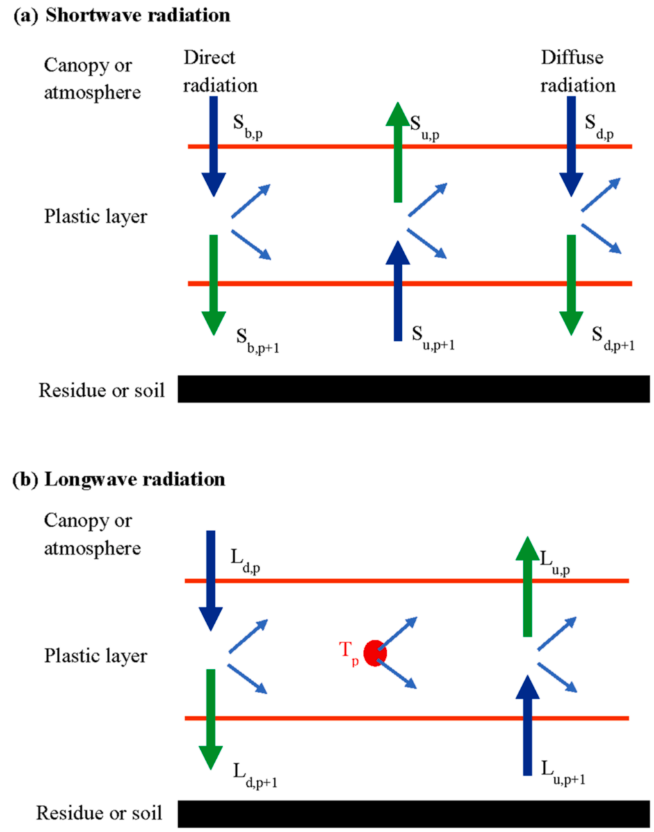

Fig. 3. Radiation transfer through a plastic layer for (a) shortwave radiation and (b) longwave radiation.

snowpack-residue-soil layered system. The new plastic mulch layer is between the snowpack and residue layers. This layer changes the shortwave and longwave radiation transfer, turbulent heat and vapor transfer from the surface, and the energy and water balances in the system. Assumptions for this submodule are as follows: (1) vapor cannot pass through the plastic material so that evaporation only occurs from uncovered areas; (2) The difference in soil temperature in the horizontal direction caused by partial mulching is ignored because RZ-SHAW is a vertical one-dimensional model; and (3) heat transfer that occurs by evaporation or condensation between the mulch and the soil surface can be ignored in comparison with the latent heat transfer between the soil and the atmosphere (Yang et al., 2012).

2.2.1. Shortwave radiation through plastic layer

Shortwave radiation exchange in the plastic layer is simulated using similar equations as the canopy layers (Eqn. [5]). Shortwave radiation exchange in the plastic layer is computed by considering downward direct (or beam, $S_{b,p}$), and upward ($S_{u,p+1}$) and downward ($S_{d,p}$) diffuse radiation being transmitted, reflected, and absorbed by the plastic layer. The upward ($S_{u,p}$) flux of diffuse shortwave radiation above the plastic layer (Fig. 3a) is computed as:

$$\begin{aligned} S_{u,p} = {} & [\tau_{d,p} + (\alpha_{d,p} f_{d,p,\downarrow\downarrow} + \tau_{d,p} f_{d,p,\downarrow\uparrow})(1-\tau_{d,p})]S_{u,p+1} \\ & +(\alpha_{d,p} f_{d,p,\downarrow\uparrow} + \tau_{d,p} f_{d,p,\downarrow\downarrow})(1-\tau_{d,p})S_{d,p} \\ & +(\alpha_{b,p} f_{b,p,\downarrow\uparrow} + \tau_{b,p} f_{b,p,\downarrow\downarrow})(1-\tau_{b,p})S_{b,p} \end{aligned} \quad [12]$$

The downward fluxes of direct ($S_{b,p+1}$) and diffuse ($S_{d,p+1}$) shortwave radiation through the plastic layer (Fig. 3a) are computed as:

$$S_{b,p+1} = \tau_{b,p} S_{b,p} \quad [13]$$

$$\begin{aligned} S_{d,p+1} = {} & [\tau_{d,p} + (\alpha_{d,p} f_{d,p,\downarrow\downarrow} + \tau_{d,p} f_{d,p,\downarrow\uparrow})(1-\tau_{d,p})]S_{d,p} \\ & +(\alpha_{b,p} f_{b,p,\downarrow\downarrow} + \tau_{b,p} f_{b,p,\downarrow\uparrow})(1-\tau_{b,p})S_{b,p} \\ & +(\alpha_{d,p} f_{d,p,\downarrow\uparrow} + \tau_{d,p} f_{d,p,\downarrow\downarrow})(1-\tau_{d,p})S_{u,p+1} \end{aligned} \quad [14]$$

where $\tau_{d,p}$ and $\tau_{b,p}$ are the transmissivity of the plastic layer to diffuse and direct (or beam) radiation, respectively. $\alpha_{b,p}$ and $\alpha_{d,p}$ are the effective albedo of the plastic layer to direct and diffuse radiation ($\alpha_{b,p} = \alpha_{d,p} = 0.14$ in this study according to Yang et al., 2012). $f_{b,p,\downarrow\uparrow}$ and $f_{d,p,\downarrow\uparrow}$ are the fractions of reflected direct and diffuse radiation scattered backward (e.g., downward radiation scattered upward), $f_{b,p,\downarrow\downarrow}$ and $f_{d,p,\downarrow\downarrow}$ are the fractions of reflected direct and diffuse radiation scattered forward. Flerchinger and Yu (2007) developed expressions for the fractions of forward and back scattered direct and diffuse radiation. The upper boundary conditions $S_{d,p}$ and $S_{b,p}$ are downward diffuse and direct radiation entering the plastic layer. The bottom boundary $S_{u,p+1}$ is the solar radiation reflected by the residue or soil layer:

$$S_{u,p+1} = \begin{cases} (1-\alpha_r)(S_{b,p+1} + S_{d,p+1}) & \text{residue under plastic} \\ (1-\alpha_s)(S_{b,p+1} + S_{d,p+1}) & \text{soil under plastic} \end{cases} \quad [15]$$

where α_r and α_s are the albedos of the residue and soil surface, respectively. Net shortwave radiation absorbed by the plastic layer ($S_{n,p}$) is computed from:

$$S_{n,p} = (1-\tau_{d,p})(S_{d,p} + S_{u,p+1}) + (1-\tau_{b,p})S_{b,p} \quad [16]$$

The transmissivities of direct and diffuse shortwave radiation for the plastic layer are calculated from:

$$\tau_{b,p} = \tau_{d,p} = (1-F_p) + \tau_p F_p \quad [17]$$

where F_p is the fraction of plastic cover (ranging from 0 to 1 with the measured value being 0.8 in this study). $\tau_p$is the transmissivity of the plastic material (0.81 in this study according to Yang et al., 2012).

2.2.2. Longwave radiation through plastic layer

The expression for upward ($L_{u,p}$) and downward ($L_{d,p+1}$) longwave radiation through the plastic layer is similar to that for shortwave radiation, but longwave emittance replaces the term for direct shortwave radiation (Fig. 3b):

$$\begin{aligned} L_{u,p} = {} & [\tau_{d,p,l} + (1-\varepsilon_p) f_{d,p,\downarrow\downarrow}(1-\tau_{d,p,l})]L_{u,p+1} \\ & +(1-\varepsilon_p) f_{d,p,\downarrow\uparrow}(1-\tau_{d,p,l})L_{d,p} \\ & +(1-\tau_{d,p,l})\varepsilon_p \sigma T_p^4 \end{aligned} \quad [18]$$

$$\begin{aligned} L_{d,p+1} = {} & [\tau_{d,p,l} + (1-\varepsilon_p) f_{d,p,\downarrow\downarrow}(1-\tau_{d,p,l})]L_{d,p} \\ & +(1-\varepsilon_p) f_{d,p,\downarrow\uparrow}(1-\tau_{d,p,l})L_{u,p+1} \\ & +(1-\tau_{d,p,l})\varepsilon_p \sigma T_p^4 \end{aligned} \quad [19]$$

where $\tau_{d,p,l}$and ε_p ($\varepsilon_p = 0.88$ in this study according to Yang et al., 2012) are transmissivity and emissivity of the plastic layer for longwave radiation, respectively. $T_p$is the temperature of the plastic layer, and σ is the Stefan-Boltzman constant. $L_{d,p}$is the downward longwave radiation from the canopy or snow above the plastic layer. $L_{u,p+1}$ is the upward flux from the residue or the soil layer below the plastic layer:

$$L_{u,p+1} = \begin{cases} (1-\varepsilon_r)L_{d,p+1} + \varepsilon_r \sigma T_r^4 & \text{residue under plastic} \\ (1-\varepsilon_s)L_{d,p+1} + \varepsilon_s \sigma T_{ss}^4 & \text{soil under plastic} \end{cases} \quad [20]$$

where ε_r and ε_s are residue and soil layer emissivity, respectively. Net longwave radiation absorbed by the plastic layer ($L_{n,p}$) is computed from:

Table 1
Measured soil physical and hydraulic parameters at various soil layers in the study site, Yangling, China.

Soil layer (cm)	Sand (%)	Silt (%)	Clay (%)	Bulk density (g cm^{-3})	Field capacity (cm^3 cm^{-3})	Wilting point (cm^3 cm^{-3})	Saturated hydraulic conductivity (cm h^{-1})	Saturated water content (cm^3 cm^{-3})
0–20	7.4	75.0	17.7	1.27	0.317	0.199	2.2	0.370
20–40	5.3	69.7	25.0	1.57	0.325	0.195	1.1	0.413
40–60	6.0	59.4	34.6	1.40	0.348	0.220	1.3	0.408
60–80	5.0	63.6	31.3	1.35	0.335	0.150	1.3	0.433
80–100	7.7	77.2	15.1	1.39	0.307	0.141	1.2	0.491

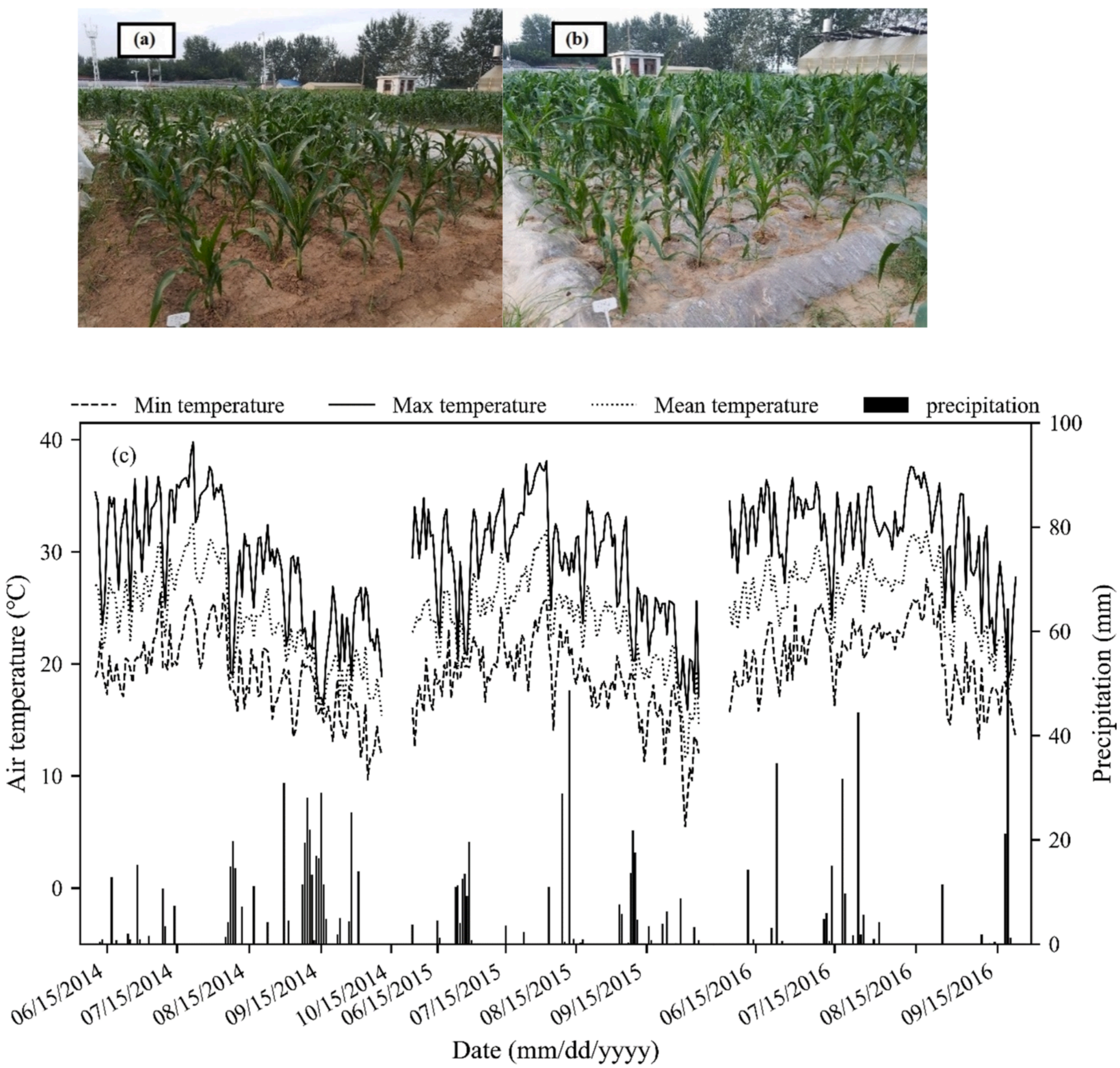

Fig. 4. Experiment field configuration and meteorological conditions: (a) a traditional planting system without mulching; (b) a planting system with full transparent plastic mulching; and (c) precipitation and air temperature during crop growing seasons (2014–2016) at Yangling, China.

Table 2
Dates of planting, harvest, irrigation, and fertilization for three years of a summer maize experiment at Yangling, China. Date format is mm/dd/yyyy.

Planting date	Harvest date	Drip irrigation date	Fertilizer application date
06/19/2014	10/11/2014	07/18/2014, 08/01/2014	06/17/2014
06/11/2015	10/08/2015	08/02/2015	06/09/2015
06/09/2016	09/22/2016	08/13/2016	06/07/2016

Table 3
Initial soil hydraulic parameter values and lower and upper boundaries used by parameter estimation software (PEST) to obtain optimized final values. BD, soil bulk density (g cm^{-3}); $\theta_{1/3}$, soil water content at 33 kPa (cm^3 cm^{-3}); θ_{15}, soil water content at 1500 kPa (cm^3 cm^{-3}); θ_s, saturated water content (cm^3 cm^{-3}); K_{sat}, saturated hydraulic conductivity (cm h^{-1}).

Layer (cm)	BD				$\theta_{1/3}$				θ_{15}	θ_s	K_{sat}
	Initial	Lower	Upper	Final	Initial	Lower	Upper	Final	Final	Final	Final
0–20	1.27	1.1	1.6	1.100	0.317	0.269	0.365	0.269	0.134	0.585	17.335
20–40	1.57	1.1	1.6	1.551	0.325	0.276	0.373	0.325	0.163	0.415	0.270
40–60	1.40	1.1	1.6	1.478	0.348	0.296	0.400	0.322	0.161	0.442	0.722
60–80	1.35	1.1	1.6	1.600	0.335	0.285	0.385	0.307	0.153	0.396	0.271
80–100	1.39	1.1	1.6	1.600	0.307	0.261	0.353	0.296	0.148	0.396	0.392

Table 4
Initial maize genetic parameter values and lower and upper boundaries used by parameter estimation software (PEST) to obtain optimized final parameter values.

Parameter[a]	Initial	Lower	Upper	Final
P1	160	100	450	246.1
P2	0.75	0.01	2	0.737
P5	780	600	1000	600
G2	750	440	1000	875.2
G3	8.5	5	16	9.207
PHINT	49	30	75	60.45
H_{max}	245	200	250	202
Biomass_half	37	30	40	30

[a] P1: Thermal time from seedling emergence to the end of juvenile phase during which the plants are not responsive to changes in photoperiod (degree days above 8 °C base temperature). P2: Extent to which development is delayed for each hour increase in photoperiod above the longest photoperiod at which development is at the maximum rate, which is considered to be 12.5 h (days). P5: Thermal time from silking to physiological maturity (degree days above 8 °C base temperature). G2: Maximum possible number of kernels per plant. G3: Grain filling rate during the linear grain filling stage and under optimum conditions (mg day^{-1}). PHINT: Phyllochron interval, the interval in thermal time (degree days) between successive leaf tip appearances. H_{max}: Maximum plant height at maturity (cm). Biomass_half: Plant biomass at half of the maximum height (g plant^{-1}).

$$L_{n,p} = \varepsilon_p(1 - \tau_{d,p,l})(L_{d,p} + L_{u,p+1} - \sigma T_p^4) \quad [21]$$

Longwave radiation transmissivity of the plastic layer is calculated as follows with an assumption that longwave radiation cannot be transmitted through plastic:

$$\tau_{d,p,l} = 1 - F_p \quad [22]$$

The model assumes no longwave radiation transfer through the plastic layer when it is covered by snow. Alternatively, the thermal conductivity of the snow is used for heat transfer through the plastic layer voids.

2.2.3. Turbulent vapor transfer through plastic layer

We assumed that vapor cannot pass through plastic material, so the vapor transfer through the non-plastic covered surface is calculated as:

$$E_p = \frac{\rho_{v,r/ss} - \rho_{v,a/c/sn}}{r_v}(1 - F_p) \quad [23]$$

where E_p is the vapor transfer through the plastic layer, $\rho_{v,/r/ss}$ is the vapor density of the residue or soil surface below the plastic layer and $\rho_{v,a/c/sn}$ is vapor density of the ambient air, plant canopy, or snow above the plastic.

2.2.4. Energy balance equation of plastic layer

Heat flux through the plastic layer considers a partial plastic mulch cover where heat fluxes represent a weighing of the areas covered by plastic and the exposed residue or soil surface layer. For the heat transport processes in the plastic layer, the energy balance equation is expressed as:

$$C_p\frac{\partial T_p}{\partial t} = \frac{\partial}{\partial z}\left(k_p\frac{\partial T_p}{\partial z}\right) - L_v\frac{\partial}{\partial z}\left(\frac{-\rho_p}{r_p}\right) + \frac{\partial R_{n,p}}{\partial z} \quad [24]$$

where C_p and T_p are volumetric heat capacity (J m^{-3} K^{-1}) and temperature (°C) of the plastic layer; k_p is heat transfer coefficient of the plastic layer (W m^{-1} K^{-1}); L_v is the latent heat of vaporization of water (2.5×10^6 J kg^{-1}); ρ_p is the vapor density (kg m^{-3}) within the plastic layer; r_p is the plastic layer boundary resistance (s m^{-1}), and $R_{n,p}$ is the net all-wave downward radiation flux within the plastic layer. Heat storage and transfer coefficients in Eqn. [24] are weighted based on the area covered by plastic mulch.

A constant volumetric specific heat capacity ($C_p = 1.2 \times 10^6$ J m^{-3} K^{-1}) of the plastic layer was used in this study, which is the product of the heat capacity of the plastic material (1000 J kg^{-1} K^{-1}) and plastic density in the layer (1200 kg m^{-3}). k_p is the weighted average of the thermal transfer coefficient of plastic covered and uncovered areas:

$$k_p = (k_t + k_v)(1 - F_p) + (k_{tp} + k_{vp})F_p \quad [25]$$

where k_{tp} and k_{vp} are thermal conduction and convection coefficients for the fraction of soil covered by plastic, and k_t and k_v are thermal conduction and convection coefficients for the fraction of soil not covered by plastic. k_{vp} is calculated from the Rayleigh number (Ham and Kluitenberg, 1994; Yang et al., 2012):

$$k_{vp} = \begin{cases} k_a/D_{p-s} & \mathrm{R_a} < 1708 \text{ or } \mathrm{T}_p > T_{ss} \\ \dfrac{k_a R_a^{1/3}\mathrm{Pr}^{0.074}}{14.5D_{p-s}} & \mathrm{R_a} \geq 1708 \text{ or } \mathrm{T}_p < T_{ss} \end{cases} \quad [26]$$

where k_a is the thermal conductivity of air (0.025 W m^{-1} k^{-1} in this study), D_{p-s} is the distance between the plastic and the soil (m), Pr is the Prandtl number of air (0.75 in this study), and R_a is the Rayleigh number. The Rayleigh number can be calculated by:

$$R_a = \frac{g\beta(T_{ss} - T_p)d_r{}^3}{\alpha\nu} \quad [27]$$

where g is the acceleration of gravity (m s^{-1}); β is the thermal expansion coefficient of air (K^{-1}, 3.5 *10^{-3} in this study), ν is the kinematics viscosity (m^2 s^{-1}, 1.5 *10^{-5} in this study), and α is the thermal diffusivity (m^2 s^{-1}, 2.2 *10^{-5} in this study). The thermal conduction coefficient of plastic (k_{tp}) was 0.30 W m^{-1} K^{-1} (Kalaprasad et al., 2000) in this study. Bristow et al. (1986) and Flerchinger et al. (2003) established equations of thermal convection coefficient for the residue layer with an assumption that thermal convection through crop residue increases linearly with wind speed. Based on these results, k_v is calculated by:

$$k_v = k_a(1 + 0.007T_p)(1 + k_{rb}\mu_p) \quad [28]$$

where μ_p is the wind speed over the plastic layer. k_t is dependent largely on moisture content of the residue and calculated by:

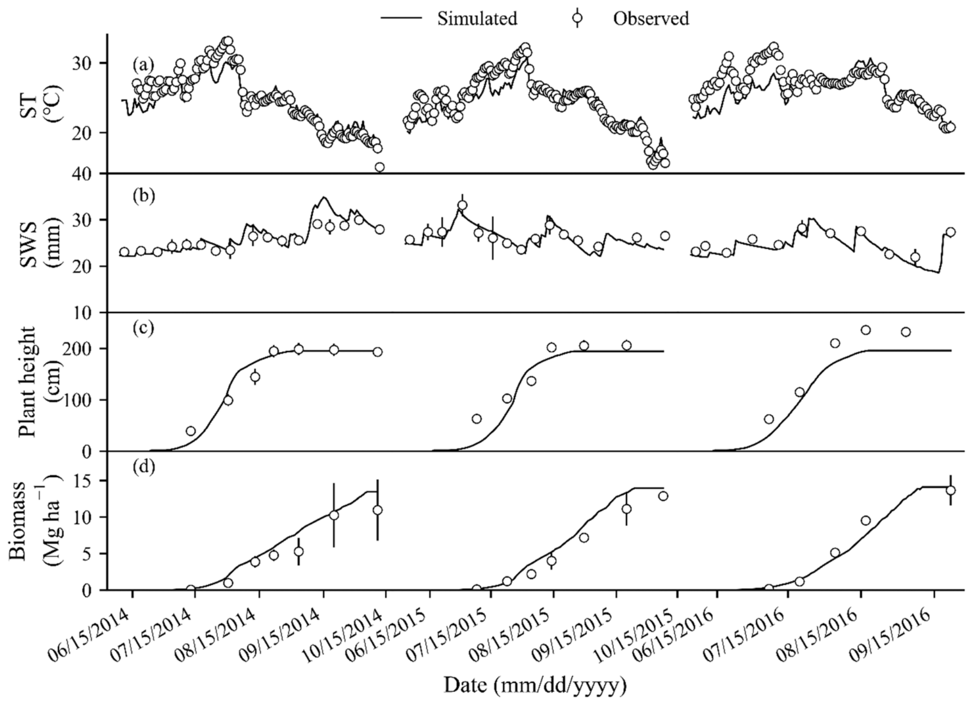

Fig. 5. RZ-SHAW model calibration with measured maize data for CK treatment during three years at Yangling, China: (a) soil temperature at 15 cm depth (ST); (b) soil water storage (SWS) in 0–100 cm layer; (c) plant height; (d) aboveground biomass. The vertical lines on the observed data symbols (b-d) designate one standard deviation around the mean (computed from three replicate plots).

Table 5
Mean difference (MD), root mean square error (RMSE), and coefficient of determination (R^2) for the simulated soil temperature at 15 cm depth (ST, °C), soil water storage (SWS, mm) in 0–100 cm layer, plant height (cm), and aboveground biomass (Mg ha^{-1}) for maize simulations by the RZ-SHAW model from 2014 to 2016 at Yangling, China.

Year	Item	ST	SWS	Plant height	Biomass
2014	MD	-0.4	0.97	1.96	1207
	RMSE	1.5	1.88	16.03	1524
	R^2	0.91	0.87	0.93	0.96
2015	MD	-0.7	-0.35	-15.42	1072
	RMSE	1.5	1.30	26.92	1334
	R^2	0.89	0.74	0.91	0.99
2016	MD	-1.1	-0.91	-32.93	-373
	RMSE	2.1	1.25	33.86	991
	R^2	0.53	0.87	0.99	0.97

$$k_t = k_l w_p(\rho_r/\rho_{rs}) + k_{rs}(\rho_r/\rho_l) \quad [29]$$

where k_l and k_{rs} are the thermal conductivities of water and residue, w_p is the water content of residue below the plastic layer, and ρ_r and ρ_{rs} are the bulk and specific densities of the residue.

2.2.5. Water balance equation of the plastic layer

Vapor flux through the plastic layer partially covering the surface is described by

$$\frac{\partial \rho_p}{\partial t} = \frac{\partial}{\partial z}(K_v \frac{\partial \rho_p}{\partial z}) + \frac{\partial}{\partial z}(\frac{-\rho_p}{r_p}) \quad [30]$$

where the three terms (kg s^{-1} m^{-3}) represent, respectively: change in vapor density within the plastic layer, net vapor flux into the plastic layer, and evaporation rate from the plastic layer. Here, K_v is the convective vapor transfer coefficient of the plastic layer (m s^{-2}), and computed as

$$K_v = \frac{k_v}{\rho_a c_a}(1 - F_p) \quad [31]$$

where k_v is thermal convection coefficient for the fraction of soil not covered by plastic calculated by Eqn. [28].

3. Materials and methods

3.1. Site and experiment description

3.1.1. Site description

The summer maize field experiment was conducted from 2014 to 2016 at the Institute of Water Saving Agriculture of Northwest A&F University, located in Yangling, Shaanxi, northwest China located on the Loess Plateau (34°20′N, 108°24′E, 521 m above mean sea level). The experiment covered three growing seasons: 11 June to 11 October 2014, 5 June to 8 October 2015, and 6 June to 22 September 2016. The experimental site was located in a region with a dry sub-humid continental monsoon climate, where summer maize is one of the major food crops. The mean annual temperature is 13.0 °C, annual average precipitation is 620 mm (mainly concentrated in July to October), mean annual evapotranspiration is approximately 884 mm, the mean annual duration of sunshine is 17,500 h (based on the data from 2008 to 2016), and the average number of frost-free days 213 d. Groundwater level at the test site was more than 5 m deep. The soil type in the experimental area is silt loam (8% sand, 73% silt, 10% clay), with a mean dry bulk density of 1.51 g cm^{-3}. The mean saturated hydraulic conductivity is 31.01 cm d^{-1} and the average saturated water content, field capacity (soil water content at 33 kpa), and permanent wilting point in volumetric values are 0.429, 0.324, and 0.189 cm^3 cm^{-3}, respectively (Ding et al., 2018). Detailed soil physical properties in the 0–100 cm soil layer are shown in Table 1. The soil is slightly alkaline with a pH of 8.32 in the surface soil (0–20 cm), and has high fertility: soil organic matter, 15.49 g kg^{-1}; microbial carbon, 166.06 mg kg^{-1}; microbial nitrogen, 14.66 mg kg^{-1}; available soil phosphorus, 19.22 mg kg^{-1}; available soil

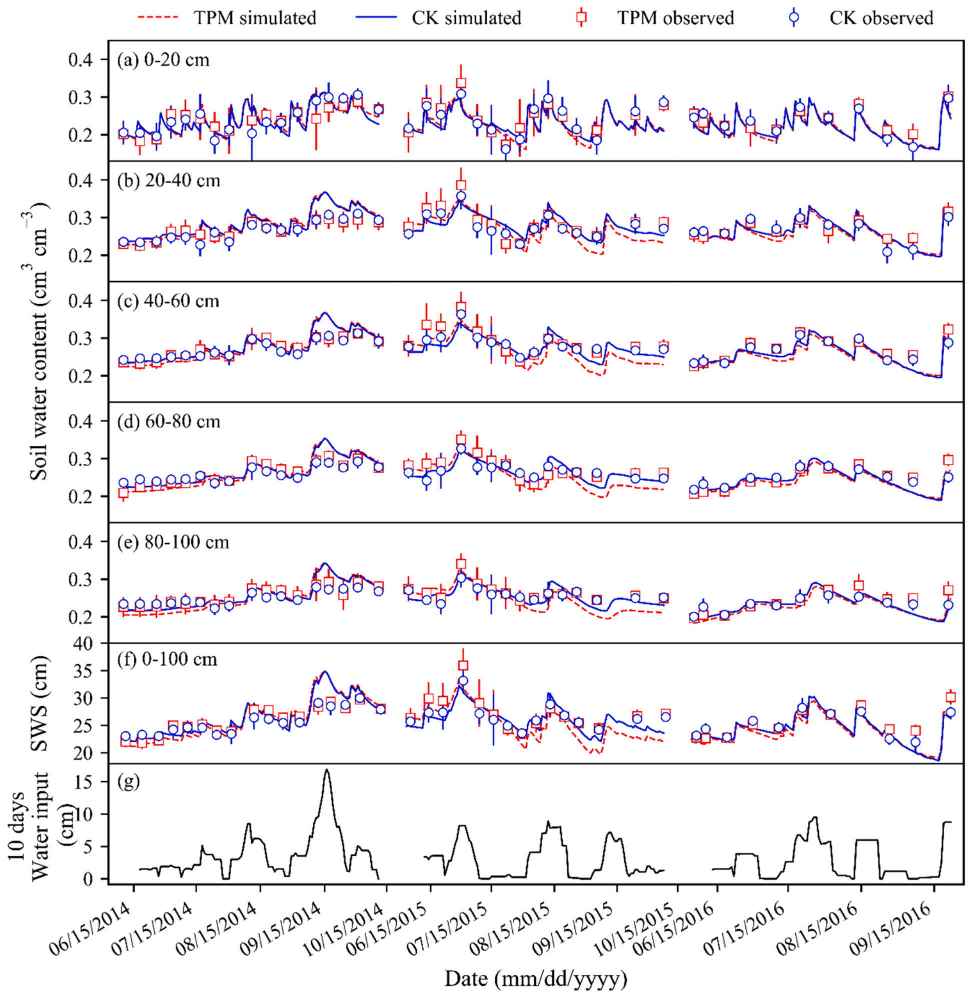

Fig. 6. Simulated and observed volumetric soil water content in different soil layers (a-e), soil water storage (SWS) in 0–100 cm layer (f), and 10-day accumulated water input (rainfall and irrigation, (g)) during maize growing seasons for CK and TPM treatments (Yangling, China, 2014–2016). The vertical lines on the observed data symbols (a-f) designate one standard deviation around the mean (computed from three replicate plots).

potassium, 132.75 mg kg^{-1}; soil NO3⁻-N, 5.19 mg kg^{-1}; and $NH4^{+}$-N, 1.31 mg kg^{-1}.

3.1.2. Experimental design

A randomized block design was used for this field experiment. Plots were planted with the summer maize variety *'qinlong 14'*. The experiment included two treatments: (1) a traditional planting system without mulching (CK, Fig. 4a), and (2) a planting system with full transparent plastic mulching (TPM, Fig. 4b). Each treatment was replicated three times using plots that were 5 m long and 2 m wide. There was a 0.5 m width guard row around each plot. Both treatments (with and without plastic mulch) used consistent management techniques (such as variety, irrigation, and fertilizer applied). Maize was planted with 60 cm row spacing and plant spacing within rows of 40 cm in June of each year during the study period. There were 52 plants (4 rows and 13 plants within row) in each plot. Nitrogen and phosphate fertilizers were surface broadcast as base fertilizer and incorporated 5 cm deep by manual tillage before planting. The types of nitrogen and phosphate fertilizers were urea and diammonium phosphate, respectively, the total amounts of pure nitrogen (N) and phosphorus (P_2O_5) were 225 kg ha^{-1} and 90 kg ha^{-1} at each application. Drip irrigation was used in the experiment and irrigated at least once during a growing season with 30 mm for each irrigation. Besides, 30 mm of water was supplied by flooding on 12 June 2015 because of extremely dry conditions at planting. Dates of planting, harvest, irrigation, and fertilization are shown in Table 2. For the TPM treatment, a transparent plastic film (0.008 mm thick) was laid over the soil surface within the plot, and holes were made in the film where seeds were planted. The plastic mulching film was removed after harvest and reestablished at the next planting date. Other field management operations, such as pest and weed control, were implemented based on local farming practices.

3.2. Sampling and measurements

The meteorological variables included daily average wind speed, minimum and maximum air temperature, relative humidity, rainfall, and sunshine duration. Data were obtained from the Yangling Meteorological Station located next to the experimental field.

The soil temperature was automatically recorded every hour (24 data points per day) using a datalogger (EM50 Datalogger, Decagon Devices, WA, USA) for each treatment during the investigation period. The thermal resistance temperature sensors (5TM) were located 15, 30, 50, 70, and 100 cm below the soil surface. The sensors' specifications can be found at https://www.metergroup.com/environment/products/ech2o-5tm-soil-moisture/.

The volumetric soil water content was observed using a Trime-TDR

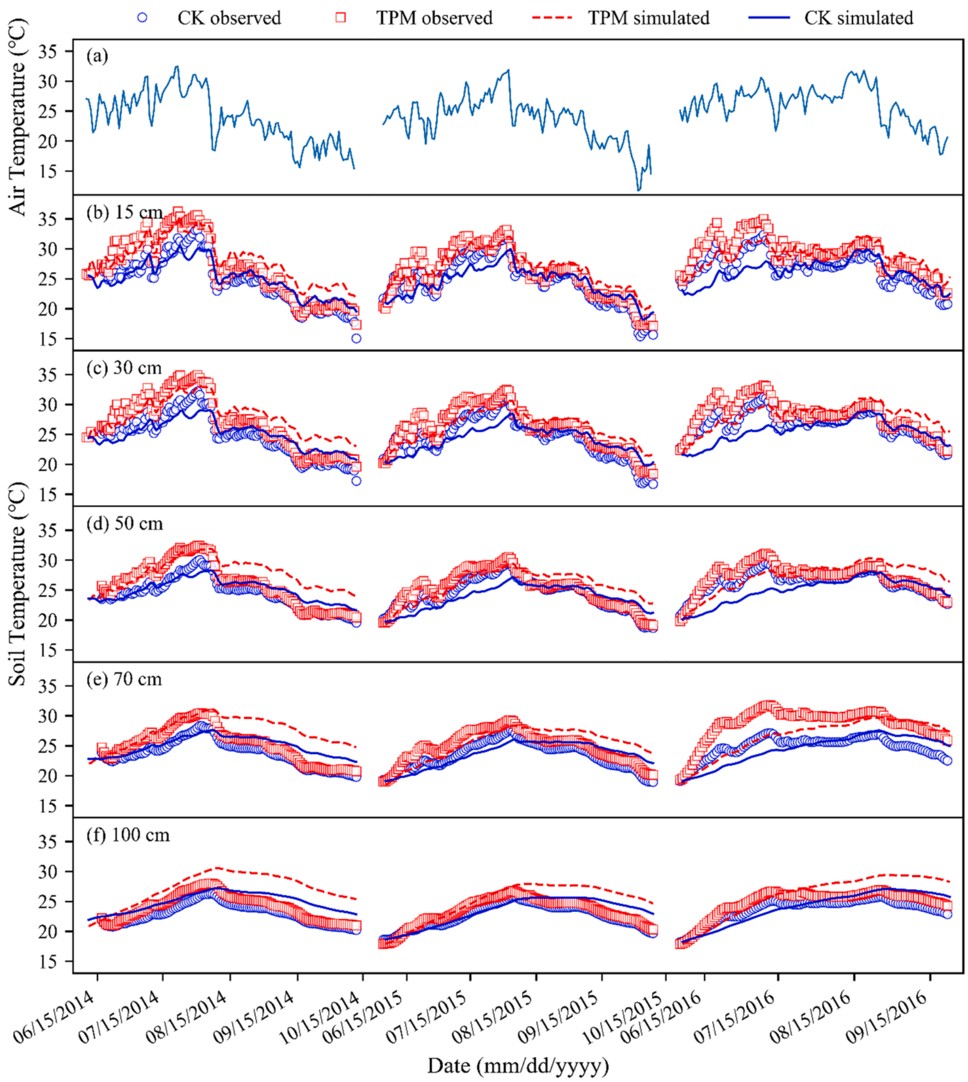

Fig. 7. Daily mean air temperature in 2014–2016 (a). Simulated and observed soil temperature for CK and TPM treatments at different soil depths ((b) 15 cm, (c) 30 cm, (d) 50 cm, (e) 70 cm, (f) 100 cm) during three maize growing seasons from 2014–2016 at Yangling, China.

device (TRIME-PICO-IPH) about every 10 days during the three maize growing seasons, and the measurements were taken from the soil surface to a 100 cm depth at 10 cm intervals. The instrument's specifications can be found at http://imko.de/en/products/soilmoisture/soil-moisture-sensors/trimepicoipht3.

Maize growth variables such as LAI, plant height, and aboveground biomass were obtained at seven different phenological stages according to Hanway (1966). For plant height and LAI, we selected two marked maize plants in each plot and observed them throughout the growing season. Plant height for each plant refers to the vertical distance from the top of the plant to the soil surface. LAI was determined by summing the lamina length × maximum width of each plant multiplied by an empirical factor of 0.75 (Eldoma et al., 2016) and then divided by the soil surface area per plant (0.192 m^2 $plant^{-1}$ was adopted in this study based on 52 plants in a 10 m^2 plot). Average plant height and LAI for each treatment were calculated as the average of three replicate plots.

Maize plant samples were randomly selected from the middle of each plot and cut at ground level to determine aboveground biomass. The plant sample should be representative of an average growth level in each plot. The selected maize plant sample was dried in an oven at 105 ℃ for 1 h and then at 75 ℃ for a minimum of 72 h until a constant weight was attained. Finally, the average aboveground biomass for each treatment was determined as the average of three replicate plots.

3.3. Data analysis method

A one-way analysis of variance (ANOVA) using the '*Statsmodels Statistics in Python*' (http://www.statsmodels.org/) was performed to test the differences between the two treatments. Multiple comparisons were made using the Tukey HSD with statistical significance denoted at the 5% level.

3.4. Model calibration and evaluation

We first calibrated the primary soil hydraulic parameters and crop cultivar parameters against the observed data of daily soil water content, soil temperature, plant height, and aboveground biomass of the CK treatment from 2014 to 2016. Initial values used were: soil hydraulic parameters based on the field measurements (Table 1) and model default crop cultivar parameters. The parameter estimation software

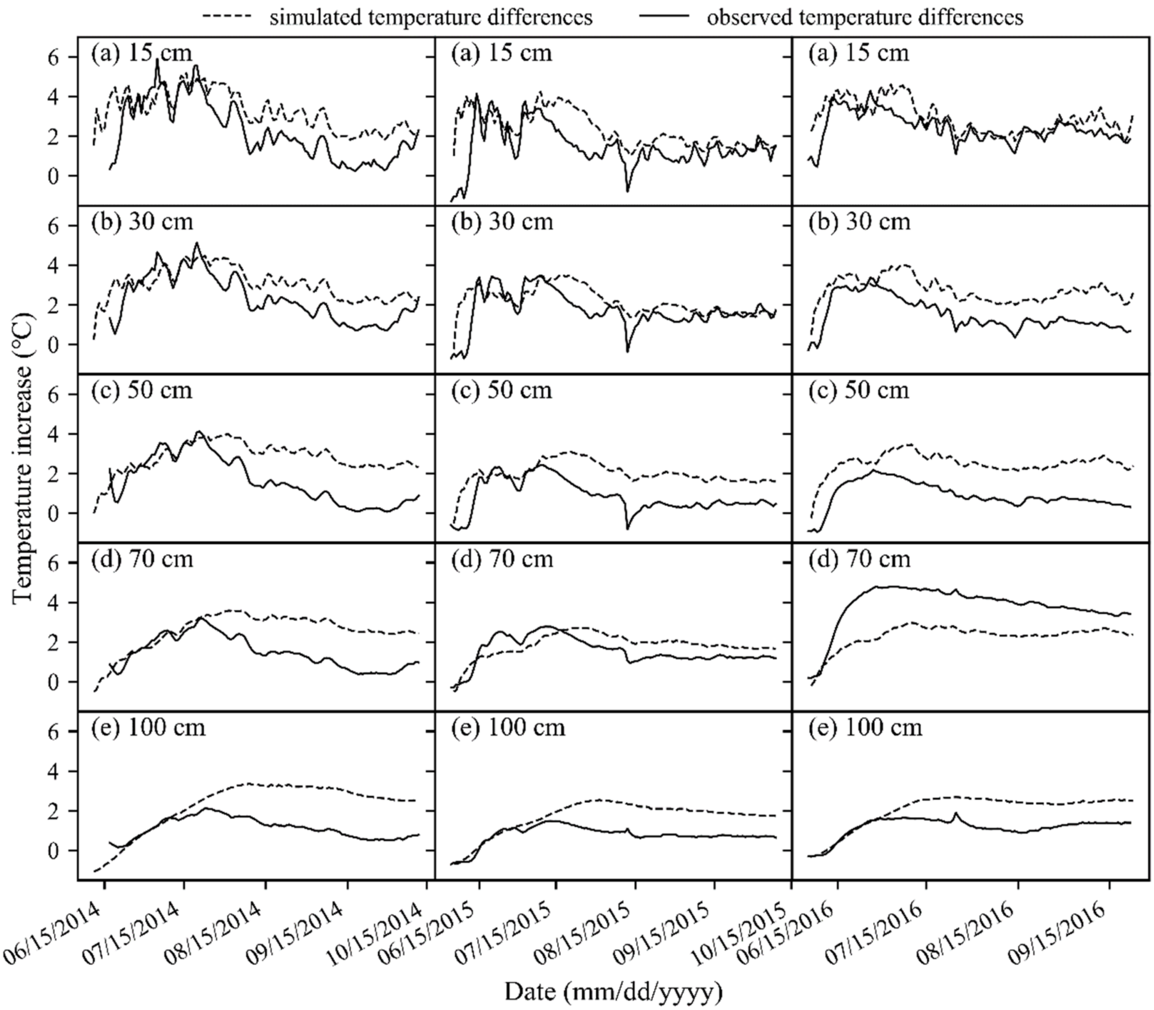

Fig. 8. Simulated temperature differences (°C) and observed temperature differences (°C) between TPM and CK treatments at 15, 30, 50, 70, 100 cm soil depths at Yangling, China. At each soil depth, temperature differences were calculated by simulated or observed soil temperature with plastic mulch minus that without plastic mulch.

(PEST; Doherty, 2004; Malone et al., 2010) was used to calibrate these parameters. During the process of parameter estimation, BD (soil bulk density) and $\theta_{1/3}$ (soil water content at 1/3 bar or 33 kPa) were limited to $\pm$ 15% of measured values. Other soil parameters were a function of calibrated parameters: θ_{15} (soil water content at 15 bar or 1500 kPa) was set as half of $\theta_{1/3}$, θ_s (saturated water content) was calculated from BD using a particle density of 2.65 g m^{-3}, and K_{sat} was calculated from θ_s and $\theta_{1/3}$ with the equation $K_{sat} = 764.5(\theta_s - \theta_{1/3})^{3.29}$ (Ahuja, 1986; Ahuja et al., 2010). Other detailed descriptions of RZWQM optimizations with PEST can be found in Fang et al. (2010a). These initial and calibrated soil hydraulic and crop genetic parameters used as inputs to the RZ-SHAW model are presented in Tables 3 and 4.

The optimized soil hydraulic and crop cultivar parameters determined for CK were also used for the TPM treatment. Observed variables for plastic mulch submodule evaluation were soil water content and temperature at the measured depths, and plant growth variables (aboveground biomass, plant height, grain yield) of TPM. The LAI required to run the model was obtained by linear interpolation of the measured values during model calibration and evaluation as shown in Thorp et al. (2010). The reason for this was to eliminate error in LAI simulation on plastic mulch effects.

The statistical indicators of Root Mean Squared Error (RMSE), Mean Difference (MD), and coefficient of determination (R^2) were used to evaluate model performance.

$$RMSE = \sqrt{\frac{1}{n}\sum_{i=1}^{n}(S_i - O_i)^2} \quad [32]$$

$$MD = \frac{1}{n}\sum_{1}^{n}(S_i - O_i) \quad [33]$$

$$R^2 = \left\{\frac{\sum_{i=1}^{n}(O_i - \overline{O})(S_i - \overline{S})}{\left[\sum_{i=1}^{n}(O_i - \overline{O})^2\right]^{0.5}\left[\sum_{i=1}^{n}(S_i - \overline{S})^2\right]^{0.5}}\right\}^2 \quad [34]$$

where S_i is the ith simulated value, O_i is the ith observed value, $\overline{S}$ and $\overline{O}$ are the average simulated and observed values, respectively, and n is the number of data pairs.

4. Results and discussion

4.1. Model calibration with CK treatment

The simulated daily soil temperature at 15 cm depth showed similar trends to the measured values, with 3-yr average RMSE of 1.7 °C (1.5 °C in 2014, 1.5 °C in 2015, and 2.1 °C in 2016) (Fig. 5a, Table 5). Soil temperature was underestimated from June to July but overestimated towards the end of the growing season in 2014–2016.

Better soil water storage simulations were obtained for 2016 than for

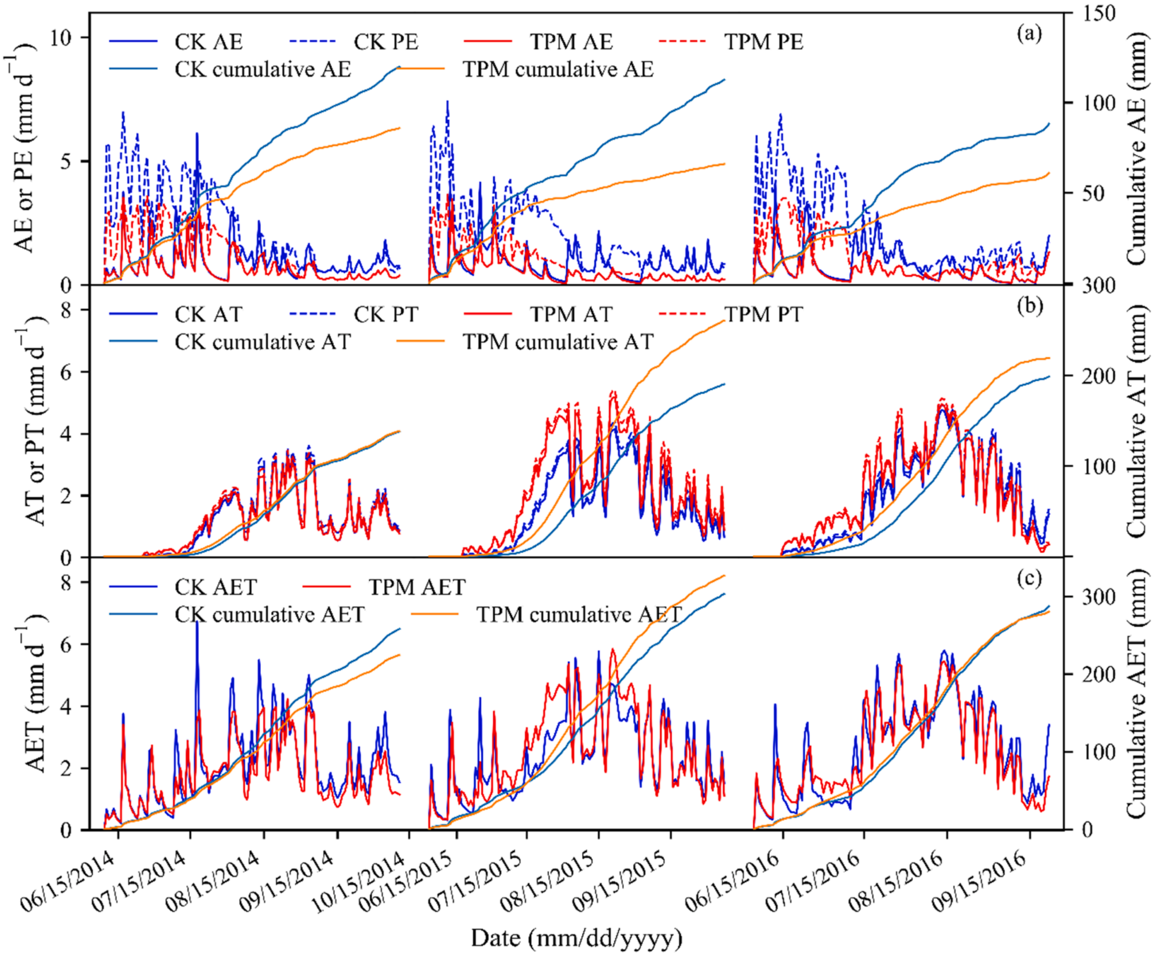

Fig. 9. Comparisons between simulated values of potential evaporation (PE), actual evaporation (AE), cumulative AE, potential transpiration (PT), actual transpiration (AT), cumulative AT, actual evapotranspiration (AET), and cumulative AET by RZ-SHAW model for two treatments (CK, TPM) during three years at Yangling, China.

2014 and 2015, with the RMSE being 1.88, 1.30 and 1.25 mm for years 2014–2016, respectively (Fig. 5b, Table 5). Soil water storage was overestimated from September to October in 2014, and underestimated in October 2015. The R^2 values for soil water storage were above 0.70 for all three years. Overall, RZ-SHAW simulated soil water dynamics well.

R^2 values for plant height during the three years were greater than 0.9, indicating that the model reasonably simulated plant height (Table 5, Fig. 5c). The simulated aboveground biomass was close to the measured data from 2014 to 2016, but better in 2016 than in 2014 and 2015 (Fig. 5d). Simulated biomass was also in good agreement with the measured values in 2014–2016 (Table 5, R^2 >0.9), with somewhat overestimation in 2014 and 2015.

In general, RZ-SHAW produced better simulations of soil water storage, soil temperature, and plant height than of biomass during the three years of the study. The simulation results of the calibrated RZ-SHAW model were considered acceptable.

4.2. Simulated and observed effects of plastic mulch on soil water content

The field-measured soil water contents at each depth were similar between the CK and TPM treatments (Fig. 6a-e). The mean observed volumetric soil moisture in the 0–100 cm soil layer during the maize growing seasons for the CK and TPM treatments were the same values (0.26 cm^3 cm^{-3} in 2014, 0.27 cm^3 cm^{-3} in 2015, 0.25 cm^3 cm^{-3} in 2016, respectively). This was mainly due to a large amount of rainfall and irrigation (Fig. 6g) in the experimental area, such that the evaporation suppression effect of the plastic mulch was not obvious.

The soil water content and soil water storage were overestimated for both CK and TPM treatments during the later part of the 2014 growing season but were underestimated in 2015 and 2016. However, the model did capture the differences in soil moisture content between CK and TPM early in 2014 and early 2015 (Fig. 6a-e). Similarly, simulated soil profile water contents followed measured values closely for both TPM and CK treatments, and correctly reflect plastic mulching effects. The RMSE between simulated and observed soil water content for TPM ranged from 0.017 to 0.030 cm^3 cm^{-3} with a mean value of 0.024 cm^3 cm^{-3} in all soil layers. The R^2 values (coefficients of determination) for TPM were greater than 0.70 in most soil layers.

4.3. Simulated and observed effects of plastic mulch on soil temperature

The observed soil temperature for TPM was higher than for CK at each soil depth in all three years (Fig. 7b-f; Fig. 8a-e). The 3-yr average soil temperatures for TPM and CK were 27.4 and 25.3 ℃ at 15 cm, 27.1 and 25.4 ℃ at 30 cm, 26.2 and 25.0 ℃ at 50 cm, 25.0 and 24.0 ℃ at 70 cm, and 24.1 and 23.1 ℃ at 100 cm, respectively. Soil temperatures decreased with increasing soil depth for both CK and TPM treatments, and the temperature differences between the CK and TPM treatments for the 15 and 100 cm depths were 2.3 and 3.3 ℃, respectively. Thus, plastic mulch increased soil temperature at all depths and increased the temperature gradient between the soil surface and deeper soil layers.

During each of the three growing seasons, the observed temperature differences between TPM and CK was greater in the early growth stages

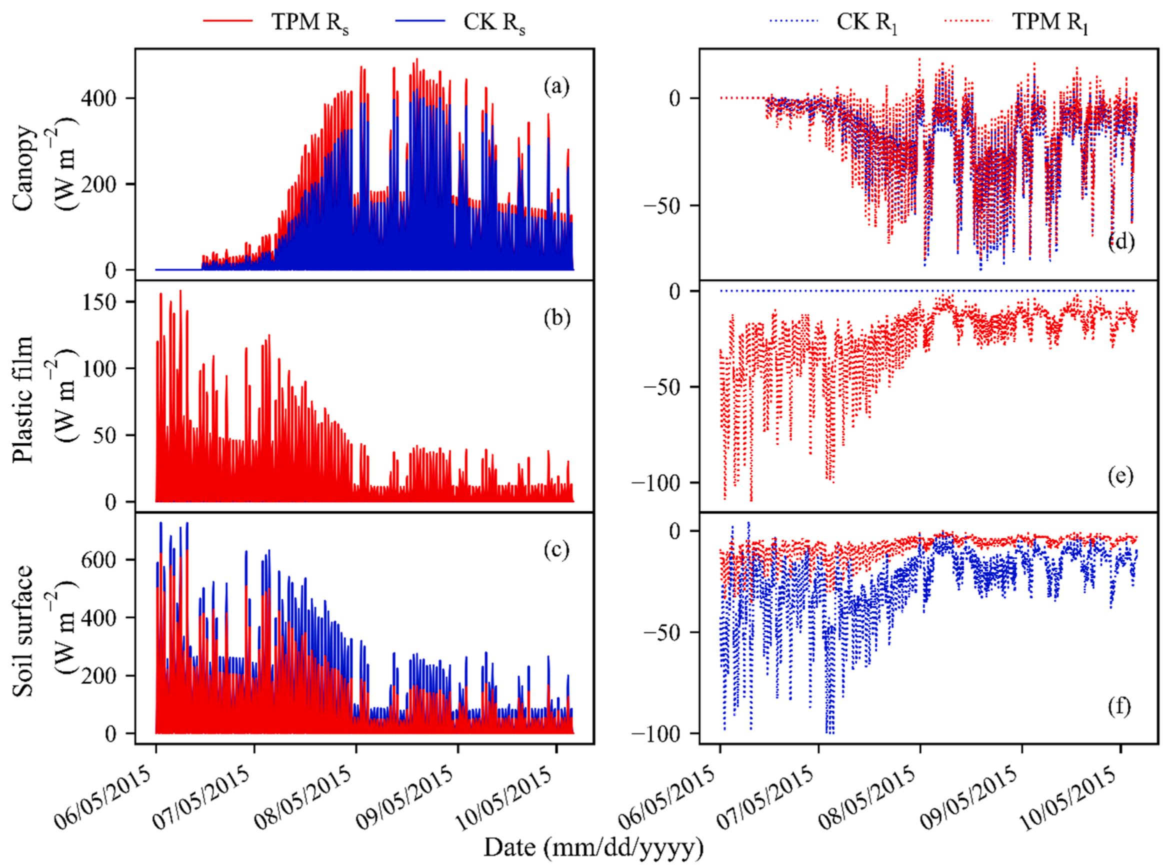

Fig. 10. Simulated shortwave radiation (R_s, column 1) and longwave radiation (R_l, column 2) at the top of the maize canopy, at the plastic film, and at the soil surface for TPM and CK treatments during the 2015 maize growing season at Yangling, China. The y-axis labels of column 2 are the same as column 1.

than that in the later period, and reached a maximum on 20 July 2014 (31 days after planting), 9 July 2015 (28 days after planting), and 26 June 2016 (17 days after planting) at the 15 cm depth (Fig. 8a). This was a result of the greater soil heat flux for TPM than for CK in the early growth stages, and less plastic mulch treatment effect in the middle and later growth stages. The average temperature differences between the two treatments generally decreased with increasing soil depth. The 3-yr average differences at 15, 30, 50, 70, and 100 cm were 2.1, 1.7, 1.2, 1.0, and 1.0 ℃, respectively.

The revised RZ-SHAW model simulated soil temperature for TPM better during early growth stages for all three years and overestimated soil temperature during the later stages. This pattern became more apparent at deeper soil depths (compare Fig. 7b to 7f). However, RZ-SHAW underestimated the decline in soil temperature for both CK and TPM treatments when air temperature decreased (for example, see the large air temperature drops on 5 August 2014, 5 August 2015, and 15 July 2015 in Fig. 7), especially at 70 and 100 cm depths. The simulated 3-yr average soil temperatures for TPM and CK were 27.9 and 25.2 ℃ at 15 cm, 27.4 and 24.9 ℃ at 30 cm, 26.9 and 24.6 ℃ at 50 cm, 26.5 and 24.3 ℃ at 70 cm, and 26.1 and 24.1 ℃ at 100 cm, respectively. Therefore, the RZ-SHAW model correctly simulated the warming effect of plastic mulch (Fig. 8) and the pattern of soil temperature decreasing with increasing soil depth. However, the simulated average soil temperatures for TPM were slightly higher than the observed values in each soil depth. The observed and simulated 3-yr average soil temperatures for TPM were 27.4 and 27.9 ℃ (difference of 0.5 ℃) at 15 cm, 27.1 and 27.4 ℃ (difference of 0.3 ℃) at 30 cm, 26.2 and 26.9 ℃ (difference of 0.7 ℃) at 50 cm, 25.0 and 26.5 ℃ (difference of 1.5 ℃) at 70 cm, and 24.1 and 26.1 ℃ (difference of 2.0 ℃) at 100 cm, respectively. The average RMSE value between simulated and observed soil temperatures for TPM was 2.3 ℃ and R^2 values were greater than 0.70 at most soil depths, which indicates that RZ-SHAW acceptably simulated soil temperatures under plastic mulch.

The simulated temperature increase caused by plastic mulch was similar to observed increases during early growth stages, but the simulated increase was greater than observed during the middle and later periods (Fig. 8). The 3-yr average simulated increases were 2.7, 2.5, 2.3, 2.2 and 2.0 ℃ at the 15, 30, 50, 70, and 100 cm soil depths, respectively, with a mean value was 2.3 ℃ over the entire 100-cm profile. The 3-yr average observed soil temperature increases were 2.1, 1.7, 1.2, 1.0 and 1.0 ℃ at 15, 30, 50, 70, and 100 cm, respectively, with a mean value was 1.4 ℃ for the soil profile. The decreased effectiveness in warming of the observed temperatures at depth may be due to the edge effects of the plot. The revised RZ-SHAW model, therefore, was able to capture the warming effect of the TPM treatment particularly at the surface but did overestimate the warming effect by a mean value of 0.9 ℃. Greater simulated soil temperature differences between the treatments than observed during the later period is probably due to overestimating G under plastic mulch conditions.

4.4. Simulated effects of plastic mulch on evapotranspiration

Plastic mulch affects the actual evaporation (AE) by reducing potential evaporation (PE). Because the plastic mulch provides a physical barrier to water vapor transfer (Eqn.[23]), simulated daily PE with the TPM treatment was lower than for CK during the entire growing period in all three years (Fig. 9a). Simulated PE differences between CK and TPM occurred in the early growth stages due to the greater canopy coverage in the later growth stages, resulting in less radiation penetrating the maize canopy to the soil surface for evaporating soil water. Cumulative PE for TPM over the three years was 158, 111, and 128 mm, which was 44%, 56%, and 47% lower than CK (284, 254 and 241 mm).

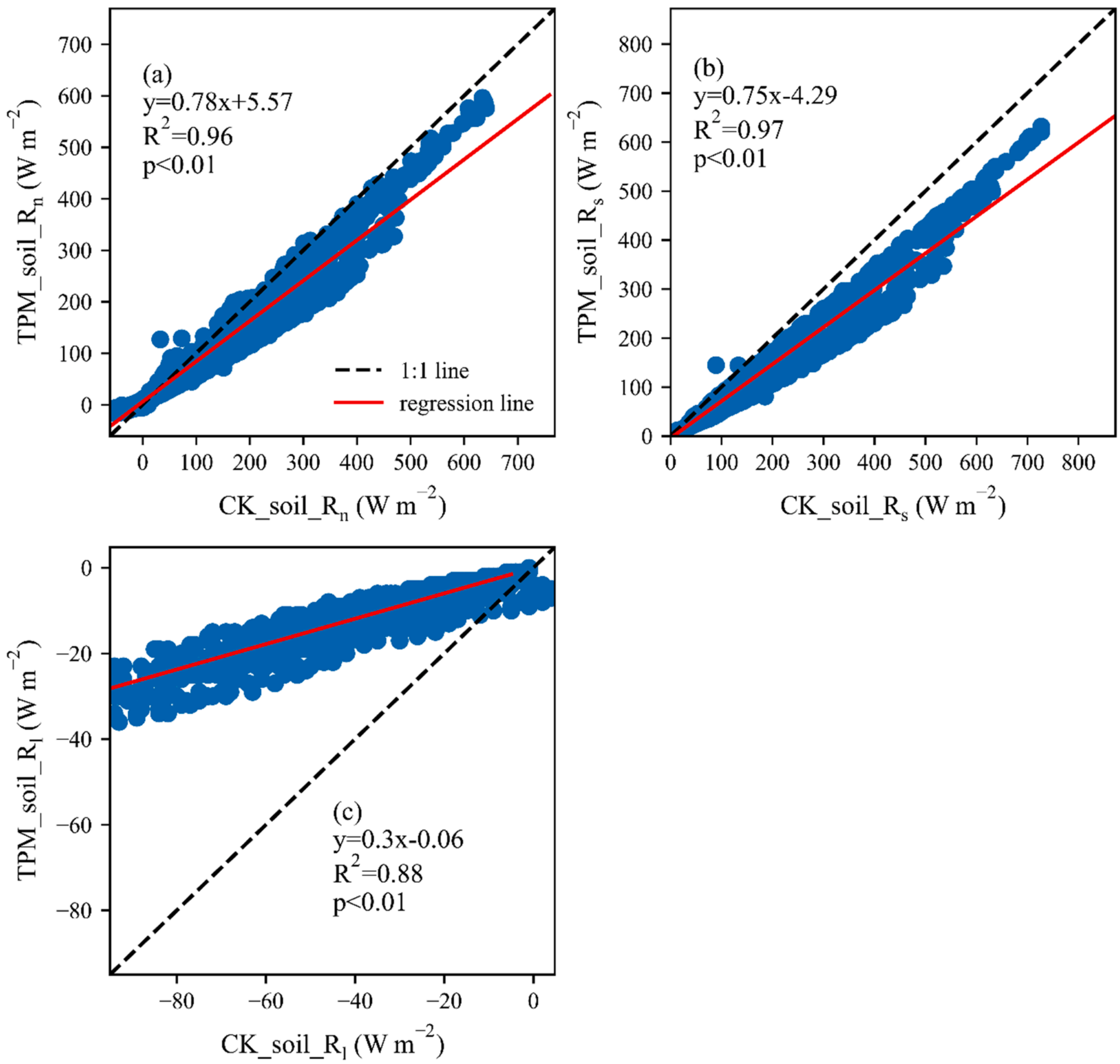

Fig. 11. Simulated hourly (a) soil net radiation (soil_R_n), (b) soil net shortwave radiation (soil_R_s), and (c) soil net longwave radiation (soil_R_l) for CK vs. TPM treatments during the 2015 maize growing season at Yangling, China.

Soil water storage was insufficient to meet PE demand, leading to lower AE than PE for both CK and TPM treatments (Fig. 9a). Simulated AE of TPM was lower than CK for most of the growing season during all three years, however, AE of TPM was higher than that of CK when the surface soil moisture content of CK was lower than that of TPM. Although there was a high PE capacity with CK during these times, there was not enough water for evaporation. Cumulative AE for TPM was 86, 66, and 61 mm, which decreased by 28%, 42%, and 31%, respectively, compared with CK (120, 113 and 88 mm) during the three growing seasons (2014–2016). Gong et al. (2017) also concluded that plastic mulch reduced total growing season evaporation compared with no mulched treatment. Differences in the effect of plastic mulching on AE over the three years indicate that the plastic mulch's effects on evaporation vary with soil moisture conditions (affected by rainfall, irrigation, etc.) and climatic conditions (interannual, regional differences).

There was little difference between potential transpiration (PT) and actual transpiration (AT) for both treatments (Fig. 9b), indicating that soil moisture was not a limiting factor for transpiration. The average daily AT values for TPM were 91%, 94%, and 94% of PT for TPM for 2014, 2015, and 2016, respectively. The corresponding average daily AT values for CK were 91%, 92%, and 94% of PT for CK. PT for TPM was nearly identical to that for CK in 2014, and higher than CK in 2015 and 2016. The PT difference between the two mulch treatments was related to measured differences in LAI, with greater LAI in the TPM treatment resulting in greater PT in 2015 and 2016. Cumulative PT of TPM was 153, 279, and 232 mm, which was 1%, 35%, and 9% greater than simulated PT of CK (152, 206 and 212 mm) for 2014, 2015, and 2016, respectively. Similarly, cumulative AT of TPM was 139, 261, and 219 mm, which was 1%, 37%, and 10% greater than CK (138, 190 and 199 mm) in 2014, 2015, and 2016, respectively.

Cumulative AET with TPM was 225, 327, and 280 mm, which was 13% less, 8% greater, and 2% less than the cumulative AET with CK (258, 303 and 287 mm) for 2014, 2015, and 2016, respectively (Fig. 9c). Gong et al. (2017) and Fan et al. (2017) reported that plastic mulch decreased AET due to the shortened growth period, while Wu et al. (2017) reported that plastic mulch increased AET due to better soil water conditions and improved maize growth. Their results indicated that the higher AET values for TPM compared to CK were reasonable.

Many production systems in China use plastic mulch to reduce evaporation, and it has been proven to be effective (Gong et al., 2017; Zhang et al., 2018b). Simulations with the RZ-SHAW model can better reflect the decrease in soil evaporation that occurs with the use of plastic mulch. Both the simulated evaporation rate and the seasonal evaporation total were seen to be lower with the plastic mulch treatment than

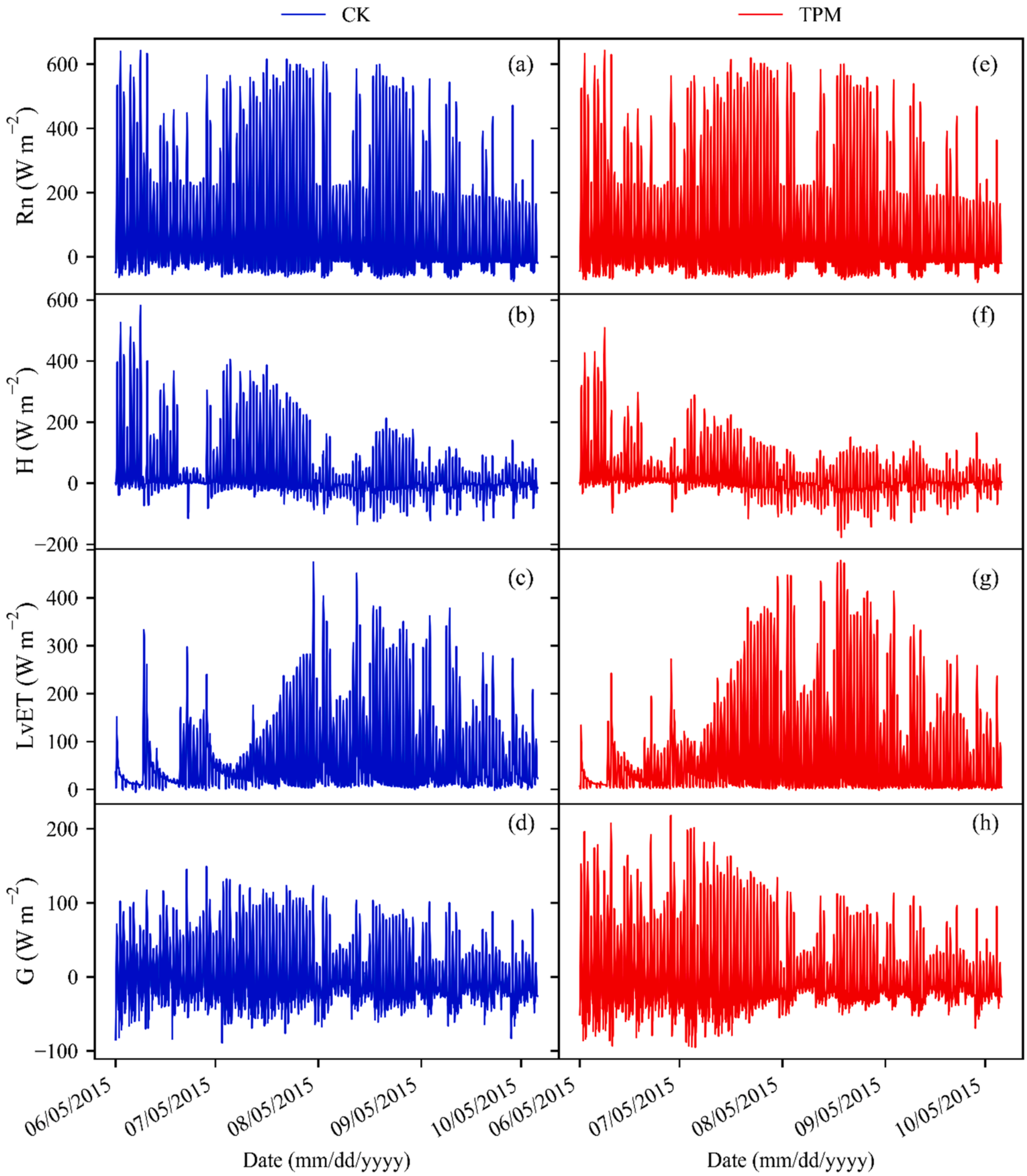

Fig. 12. The simulated energy components including net radiation (R_n), sensible heat flux (H), latent heat flux (L_vET), and soil heat flux (G) for TPM and CK treatments during the 2015 maize growing season at Yangling, China.

with the non-mulched treatment during the three years (Fig. 9). However, some studies have shown that plastic mulch can improve LAI and increase transpiration (Zhang et al., 2018b). Thus, total seasonal ET may be larger or smaller with plastic mulch compared to that without mulch depending on the reduction in surface evaporation and the change in the fraction of total ET that is transpiration. In this study, the simulated seasonal transpiration with plastic mulch was similar (2014) or larger (2015 and 2016) than with the CK treatment, which was commensurate with measured LAI and soil water content conditions in all three years of the study. Some previous studies have shown that plastic mulch can reduce total evapotranspiration compared with a non-mulched treatment (Gong et al., 2017; Li et al., 2018; Zhang et al., 2018b). The reasons for that result were either that plastic mulch can accelerate the growth process and shorten the growth period, or that evaporation reduction is greater than transpiration increase. However, some studies have shown that evapotranspiration with plastic mulch was greater than with non-mulched conditions (Chen et al., 2015; Li et al., 2013a). These different results among previous studies may be caused by local differences in precipitation timing and amount during the growing season.

4.5. Simulated effects of plastic mulch on surface energy fluxes

Plastic mulch can increase substrate albedo, resulting in less simulated shortwave and longwave radiation being received by the soil surface under TPM treatment than under CK (Fig. 10c, f), which agrees with results of Chung and Horton (1987), Li et al. (2016), and Liakatas et al. (1986). Simulated soil R_n for TPM was about 78% of R_n for CK over the growing season (Fig. 11a), which is similar to the measured 80% as

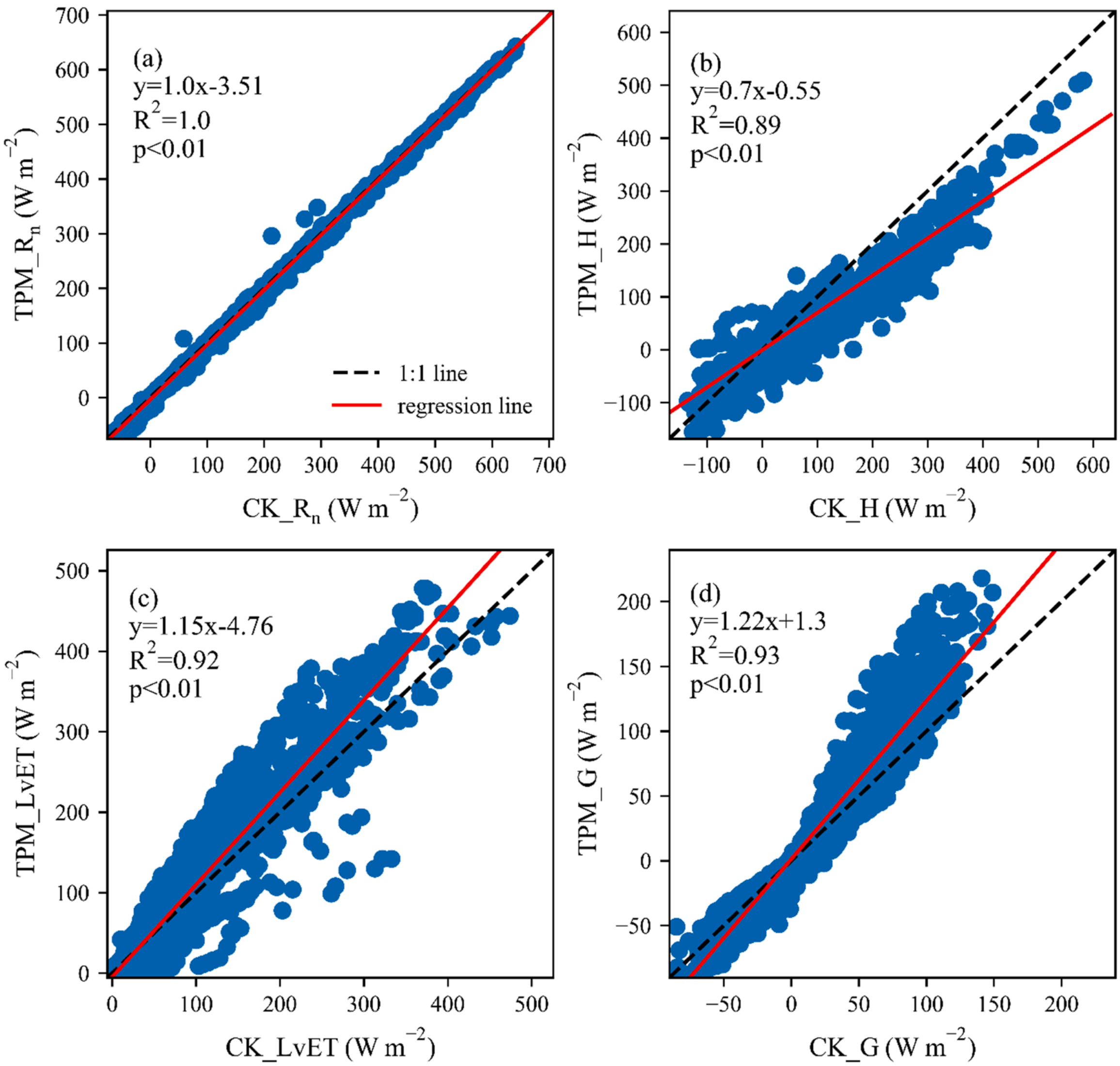

Fig. 13. Simulated hourly (a) total net radiation (R_n), (b) total sensible heat flux (H), (c) total latent heat flux (L_vET), and (d) total soil heat flux (G) for CK vs. TPM treatments during the 2015 maize growing season at Yangling, China.

reported by Li et al. (2016) for plastic mulching in a cotton field. Simulated soil R_s for TPM was about 75% of R_s for CK (Fig. 11b), which is lower than the value of 84% measured by Li et al. (2016). Li et al. (2016) reported that measured soil R_l under plastic mulch were nearly the same as CK. In contrast, our simulated values of soil R_l for TPM were about 30% of R_l for CK (Fig. 11c), suggesting that the model may have underestimated the soil R_l for TPM. However, since soil R_l was small, this underestimation of soil R_l under plastic mulch should not have a big impact on soil R_n (Fig. 11a). The difference in soil R_n between TPM and CK treatments decreased as LAI and canopy coverage increased because more radiation was intercepted by the canopy so differences in substrate albedo were less influential.

For the canopy-plastic-soil system, plastic mulch reduced simulated net radiation in the soil layer, but it also absorbed shortwave radiation (Fig. 10b) and emitted longwave radiation (Fig. 10e). Meanwhile, the denser maize canopy for TPM compared to CK intercepted more shortwave radiation (Fig. 10a). Overall, the slightly lower total seasonal R_n received by TPM (101 W m^{-2}) compared to CK (104 W m^{-2}) agrees with other previously reported results (Fan et al., 2017; Li et al., 2016). The slope of the regression between total R_n in the CK and TPM treatments was 1.0 (Fig. 13a), which compares with a smaller regression slope (0.9) between R_n in a maize field with and without plastic mulch reported by Fan et al. (2017) and Zhang et al. (2018b). We suspect, therefore, that this means RZ-SHAW may overestimate the total R_n differences between CK and TPM.

Simulated sensible heat (H) for TPM was lower than for CK (Fig. 12b, f), especially before canopy closure which occurred on 15 August. H between substrate beneath the plastic and the atmosphere first passes through the layer of still air beneath the plastic by molecular diffusion and is then transmitted above the plastic by turbulent transfer processes. The plastic mulch acts as a barrier to the direct turbulent exchange of the heated air under the mulch with air above it. The molecular diffusion coefficient is much smaller than the turbulent diffusion coefficient during energy transfer, so the sensible heat exchange of the soil under the plastic mulch is inhibited. RZ-SHAW was able to simulate this barrier effect, and the slope of the regression between H for CK and TPM was 0.7 (Fig. 13b), indicating that H for TPM was about 70% of CK during the entire growing season.

L_vET for both CK and TPM treatments showed typical seasonal variation, increasing from June to August and then decreasing slowly to harvest (Fig. 12c, g), in response to LAI. This result is likely because the L_vET for TPM mainly comes from plant transpiration. In the early growing stages from sowing to mid-July when plant transpiration is low, the barrier effect of the plastic mulch on evaporation leads to a lower

L_vET under TPM than under CK. When the maize canopy was completely closed, the contribution of evaporation to L_vET was reduced, and the effect of plastic mulch on L_vET was lessened. Therefore, the difference in L_vET between CK and TPM became less obvious during later growth stages. The average L_vET for TPM during the entire growing season was 74 W m^{-2}, which is higher than for CK (69 W m^{-2}), and Fig. 13c shows that L_vET for TPM was about 115% of L_vET for CK in 2015.

Simulated soil heat flux (G) under TPM was higher than under CK during the growing season, especially in the early part of the growing season (Fig. 12d, h), which agrees with the results of Fan et al. (2017). The average G for TPM was 4.0 W m^{-2} with a standard deviation of 56.3 W m^{-2}, while the average G for CK was 2.2 W m^{-2} with a standard deviation of 44.6 W m^{-2}, which means that the plastic mulch increased soil heat flux into deeper soil layers. The slope of the regression between G for CK and TPM treatments was 1.22 (Fig. 13d), indicating that G for TPM was about 122% of G for CK over the entire growing season. Accumulated G (positive and negative values will offset) for TPM and CK during the growing season was 12.2 KJ m^{-2} and 6.7 KJ m^{-2}, respectively. However, accumulated G before 15 August for TPM and CK were 18.0 KJ m^{-2} and 12.3 KJ m^{-2} and were − 5.9 MJ m^{-2} and − 5.7 MJ m^{-2}, respectively, after 15 August. These results indicate that the soil mainly receives heat before canopy closure, and mainly releases heat after canopy closure. Also, the increased G for TPM compared with CK was mainly due to the greater amount of heat received during the early growth stages, as G was not much different between the two treatments in the later growth stages after canopy closure.

5. Conclusions

The modified RZ-SHAW model produced reasonable simulation trends for soil water, soil temperature, evapotranspiration, and energy fluxes for the plastic mulch treatment from 2014–2016. Plastic mulch increased soil temperature about 1.0–2.1 ℃ in 0–100 cm, especially in surface soil layer during early growing season. The model was able to mimic the increased soil temperatures under the mulch treatment compared to the non-mulched treatment. Very little difference in water content was found between the treatments for either the simulated or measured values. Based on comparisons between simulated and observed values, the model was able to adequately simulate soil water content under plastic mulch at different soil depths during the three years of the study, with a mean Root Mean Square Error (RMSE) value of 0.024 cm^3 cm^{-3} in all soil layers. The model did however simulate the reduced evaporation due to mulch and the consequent transpiration increase, although measurements are not available to confirm this model observation. When simulating the use of plastic mulch, the model may overestimate R_n and G and underestimate H and L_vET, resulting in an overestimation of soil temperature.

The current modified RZ-SHAW model can be used as a decision tool for irrigation water management and automatic irrigation under plastic mulch, plastic cover ratio adjustment, optimize the parameters of the mulching film, and even explore the feasibility of maize planting in areas limited by cold temperatures.

Declaration of Competing Interest

The authors declare that they have no known competing financial interests or personal relationships that could have appeared to influence the work reported in this paper.

Acknowledgments

We are indebted to Xia Liu, Han Cao, Yan Zhang, Haojie Zhang, Jie Wang, Cheng Li, Xiaoqi Luo, Wenjie Wu, Yue Li, Xiaolian Pan for their help in data observation. This work was supported by the National Natural Science Foundation of China (Grant No. 51879224), the Coordination & Innovation Project of Science & Technology in Shaanxi (Grant No. 2016KTZDNY03-06), the 111 Project (Grant No. B12007), and the National Natural Science Foundation of China (Grant No. 51609237). We are very appreciated with the pertinent comments provided by David C. Nielsen, USDA-Agricultural Research Service, USA, which greatly improved the manuscript.

References

Ahuja, L.R., 1986. Characterization and modeling of chemical transfer to runoff. In: Stewart, B.A. (Ed.), Advances in Soil Science. Springer, New York, pp. 149–188. https://doi.org/10.1007/978-1-4613-8612-4_3.

Ahuja, L.R., Ma, L.W., Green, T.R., 2010. Effective soil properties of heterogeneous areas for modeling infiltration and redistribution. Soil Sci. Soc. Am. J. 74 (5), 1469–1482. https://doi.org/10.2136/sssaj2010.0073.

Ahuja, L.R., Rojas, K.W., Hanson, J.D., Shaffer, M.J., Ma, L.W., 2000. Root Zone Water Quality Model: Modelling Management Effects on Water Quality and Crop Production. Water Resources Publications, Highlands Ranch, Colorado.

Bristow, K.L., Campbell, G., Papendick, R., Elliott, L., 1986. Simulation of heat and moisture transfer through a surface residue—soil system. Agric. For. Meteorol. 36 (3), 193–214. https://doi.org/10.1016/0168-1923(86)90035-3.

Bu, L.D., Zhu, L., Liu, J.L., Luo, S.S., Chen, X.P., Li, S.Q., 2013. Source-sink capacity responsible for higher maize yield with removal of plastic film. Agron. J. 105 (3), 591–598. https://doi.org/10.2134/agronj2012.0459.

Campbell, G.S., Norman, J.M., 1998. An introduction to environmental biophysics, second ed. Springer-Verlag, New York. https://doi.org/10.1007/978-1-4612-1626-1.

Cavero, J., Ortega, R.G., Zaragoza, C., 1996. Clear plastic mulch improved seedling emergence of direct-seeded pepper. HortScience 31 (1), 70–73. https://doi.org/10.21273/HORTSCI.31.1.70.

Celia, M.A., Ahuja, L.R., Pinder, G.F., 1987. Orthogonal collocation and alternating-direction procedures for unsaturated flow problems. Adv. Water Res. 10 (4), 178–187. https://doi.org/10.1016/0309-1708(87)90027-3.

Celia, M.A., Bouloutas, E.T., Zarba, R.L., 1990. A general mass-conservative numerical solution for the unsaturated flow equation. Water Resour. Res. 26 (7), 1483–1496. https://doi.org/10.1029/WR026i007p01483.

Chen, Y.L., Liu, T., Tian, X.H., Wang, X.F., Li, M., Wang, S.X., Wang, Z.H., 2015. Effects of plastic film combined with straw mulch on grain yield and water use efficiency of winter wheat in Loess Plateau. Field Crop. Res. 172, 53–58. https://doi.org/10.1016/j.fcr.2014.11.016.

Chung, S., Horton, R., 1987. Soil heat and water flow with a partial surface mulch. Water Resour. Res. 23 (12), 2175–2186. https://doi.org/10.1029/WR023i012p02175.

Cosic, M., Stricevic, R., Djurovic, N., Moravcevic, D., Pavlovic, M., Todorovic, M., 2017. Predicting biomass and yield of sweet pepper grown with and without plastic film mulching under different water supply and weather conditions. Agric. Water Manag. 188, 91–100. https://doi.org/10.1016/j.agwat.2017.04.006.

Ding, D.Y., Zhao, Y., Feng, H., Hill, R.L., Chu, X.S., Zhang, T.B., He, J.Q., 2018. Soil water utilization with plastic mulching for a winter wheat-summer maize rotation system on the Loess Plateau of China. Agric. Water Manag. 201, 246–257. https://doi.org/10.1016/j.agwat.2017.12.029.

Doherty, J., 2004. PEST: Model-Independent Parameter Estimation User Manual, fifth ed. Watermark Numerical Computing, Brisbane, Australia.

Eldoma, I.M., Li, M., Zhang, F., Li, F.M., 2016. Alternate or equal ridge–furrow pattern: Which is better for maize production in the rain-fed semi-arid Loess Plateau of China? Field Crop. Res. 191, 131–138. https://doi.org/10.1016/j.fcr.2016.02.024.

Fan, Y.Q., Ding, R.S., Kang, S.Z., Hao, X.M., Du, T.S., Tong, L., Li, S., 2017. Plastic mulch decreases available energy and evapotranspiration and improves yield and water use efficiency in an irrigated maize cropland. Agric. Water Manag. 179, 122–131. https://doi.org/10.1016/j.agwat.2016.08.019.

Fang, Q.X., Green, T.R., Ma, L.W., Erskine, R.H., Malone, R.W., Ahuja, L.R., 2010a. Optimizing soil hydraulic parameters in RZWQM2 under fallow conditions. Soil Sci. Soc. Am. J. 74 (6), 1897–1913. https://doi.org/10.2136/sssaj2009.0380.

Fang, Q.X., Ma, L.W., Flerchinger, G.N., Qi, Z., Ahuja, L.R., Xing, H.T., Li, J., Yu, Q., 2014a. Modeling evapotranspiration and energy balance in a wheat–maize cropping system using the revised RZ-SHAW model. Agric. For. Meteorol. 194, 218–229. https://doi.org/10.1016/j.agrformet.2014.04.009.

Fang, Q.X., Ma, L.W., Nielsen, D.C., Trout, T.J., Ahuja, L.R., 2014b. Quantifying corn yield and water use efficiency under growth stage–based deficit irrigation conditions. In: Ahuja, L.R., Ma, L., Lascano, R.J. (Eds.), Practical Applications of Agricultural System Models to Optimize the Use of Limited Water. American Society of Agronomy, Inc., Crop Science Society of America, Inc., and Soil Science Society of America, Inc., Madison, WI, pp. 1–24. https://doi.org/10.2134/advagricsystmodel5.c1.

Fang, Q.X., Ma, L.W., Yu, Q., Ahuja, L.R., Malone, R.W., Hoogenboom, G., 2010b. Irrigation strategies to improve the water use efficiency of wheat–maize double cropping systems in North China Plain. Agric. Water Manag. 97 (8), 1165–1174. https://doi.org/10.1016/j.agwat.2009.02.012.

Flerchinger, G.N., 2017. The Simultaneous Heat and Water (SHAW) model: Technical Documentation, Version 3.0. USDA-ARS Northwest Watershed Research Center, Boise, Idaho. 〈https://www.ars.usda.gov/ARSUserFiles/20520500/SHAW/ShawDocumentation.30.pdf〉.

Flerchinger, G.N., Pierson, F.B., 1991. Modeling plant canopy effects on variability of soil temperature and water. Agric. For. Meteorol. 56 (3), 227–246. https://doi.org/10.1016/0168-1923(91)90093-6.

Flerchinger, G.N., Sauer, T.J., Aiken, R.A., 2003. Effects of crop residue cover and architecture on heat and water transfer at the soil surface. Geoderma 116 (1–2), 217–233.

Flerchinger, G.N., Saxton, K.E., 1989. Simultaneous heat and water model of a freezing snow-residue-soil system i. Theory and development. Trans. ASABE 32 (2), 565–0571. https://doi.org/10.13031/2013.31040.

Flerchinger, G.N., Xiao, W., Sauer, T.J., Yu, Q., 2009. Simulation of within-canopy radiation exchange. NJAS - Wagening. J. Life Sci. 57 (1), 5–15. https://doi.org/10.1016/j.njas.2009.07.004.

Flerchinger, G.N., Yu, Q., 2007. Simplified expressions for radiation scattering in canopies with ellipsoidal leaf angle distributions. Agric. For. Meteorol. 144 (3), 230–235. https://doi.org/10.1016/j.agrformet.2007.03.002.

Fuchs, M., Campbell, G., Papendick, R., 1978. An analysis of sensible and latent heat flow in a partially frozen unsaturated soil. Soil Sci. Soc. Am. J. 42 (3), 379–385. https://doi.org/10.2136/sssaj1978.03615995004200030001x.

Gong, D.Z., Mei, X.R., Hao, W.P., Wang, H.B., Caylor, K.K., 2017. Comparison of ET partitioning and crop coefficients between partial plastic mulched and non -mulched maize fields. Agric. Water Manag. 181, 23–34. https://doi.org/10.1016/j.agwat.2016.11.016.

Guo, D.X., Chen, C.F., Guo, P.Y., Yuan, X.Y., Xing, X.G., Ma, X.Y., 2018. Evaluation of AquaCrop model for foxtail millet (*Setaria italica*) growth and water use with plastic film mulching and no mulching under different weather conditions. Water 10 (7), 1–17. https://doi.org/10.3390/w10070836.

Ham, J.M., Kluitenberg, G., 1994. Modeling the effect of mulch optical properties and mulch-soil contact resistance on soil heating under plastic mulch culture. Agric. Meteorol. 71 (3–4), 403–424. https://doi.org/10.1016/0168-1923(94)90022-1.

Han, J., Jia, Z.K., Wu, W., Li, C.S., Han, Q.F., Zhang, J., 2014. Modeling impacts of film mulching on rainfed crop yield in Northern China with DNDC. Field Crop. Res. 155, 202–212. https://doi.org/10.1016/j.fcr.2013.09.004.

Hanway, J.J., 1966. How a Corn Plant Develops. Special Report. 38. Iowa Agricultural and Home Economics Experiment Sration Publications: Iowa State University of Science and Technology Cooperative Extension Service Ames,. ⟨http://lib.dr.iastate.edu/specialreports/38⟩.

Huang, D., Han, J.G., Wu, W.L., Wu, J.Y., 2008. Soil temperature effects on emergence and survival of Iris lactea seedlings. N. Z. J. Crop Hortic. Sci. 36 (3), 183–188. https://doi.org/10.1080/01140670809510234.

Jones, J.W., Hoogenboom, G., Porter, C.H., Boote, K.J., Batchelor, W.D., Hunt, L., Wilkens, P.W., Singh, U., Gijsman, A.J., Ritchie, J.T., 2003. The DSSAT cropping system model. Eur. J. Agron. 18 (3–4), 235–265. https://doi.org/10.1016/S1161-0301(02)00107-7.

Kalaprasad, G., Pradeep, P., Mathew, G., Pavithran, C., Thomas, S., 2000. Thermal conductivity and thermal diffusivity analyses of low-density polyethylene composites reinforced with sisal, glass and intimately mixed sisal/glass fibres. Compos. Sci. Technol. 60 (16), 2967–2977. https://doi.org/10.1016/S0266-3538(00)00162-7.

Li, F.M., Guo, A.H., Wei, H., 1999. Effects of clear plastic film mulch on yield of spring wheat. Field Crop. Res. 63 (1), 79–86. https://doi.org/10.1016/S0378-4290(99)00027-1.

Li, N.N., Tian, F.Q., Hu, H.C., Lu, H., Ming, G.H., 2016. Effects of plastic mulch on soil heat flux and energy balance in a cotton field in northwest China. Atmosphere 7 (8). https://doi.org/10.3390/atmos7080107.

Li, R., Hou, X.Q., Jia, Z.K., Han, Q.F., Ren, X.L., Yang, B.P., 2013a. Effects on soil temperature, moisture, and maize yield of cultivation with ridge and furrow mulching in the rainfed area of the Loess Plateau, China. Agric. Water Manag. 116, 101–109. https://doi.org/10.1016/j.agwat.2012.10.001.

Li, S.E., Kang, S.Z., Zhang, L., Ortega-Farias, S., Li, F.S., Du, T.S., Tong, L., Wang, S.F., Ingman, M., Guo, W.H., 2013b. Measuring and modeling maize evapotranspiration under plastic film-mulching condition. J. Hydrol. 503, 153–168. https://doi.org/10.1016/j.jhydrol.2013.07.033.

Li, S.Y., Li, Y., Lin, H.X., Feng, H., Dyck, M., 2018. Effects of different mulching technologies on evapotranspiration and summer maize growth. Agric. Water Manag. https://doi.org/10.1016/j.agwat.2017.10.025.

Li, Z.Z., Ma, L.W., Flerchinger, G.N., Ahuja, L.R., Wang, H., Li, Z.S., 2012. Simulation of overwinter soil water and soil temperature with SHAW and RZ-SHAW. Soil Sci. Soc. Am. J. 76 (5), 1548–1563. https://doi.org/10.2136/sssaj2011.0434.

Liakatas, A., Clark, J., Monteith, J., 1986. Measurements of the heat balance under plastic mulches. Part I. Radiation balance and soil heat flux. Agric. For. Meteorol. 36 (3), 227–239. https://doi.org/10.1016/0168-1923(86)90037-7.

Liang, H., Hu, K.L., Qin, W., Zuo, Q., Zhang, Y.N., 2017. Modelling the effect of mulching on soil heat transfer, water movement and crop growth for ground cover rice production system. Field Crop. Res. 201, 97–107. https://doi.org/10.1016/j.fcr.2016.11.003.

Loro, 2014. China invests in land and research in Africa, South America, Central Asia to feed the world's largest population. YaleGlobal Online. Yale University. ⟨https://yaleglobal.yale.edu/content/chinese-agriculture-goes-global#:~:text=avocados%20and%20blueberries.-,China%20is%20home%20to%2022%20percent%20of%20the%20world's%20population,pollution%20of%20rivers%20and%20lakes⟩.

Ma, L., Trout, T.J., Ahuja, L.R., Bausch, W.C., Saseendran, S.A., Malone, R.W., Nielsen, D. C., 2012a. Calibrating RZWQM2 model for maize responses to deficit irrigation. Agric. Water Manag. 103 (Supplement C), 140–149. https://doi.org/10.1016/j.agwat.2011.11.005.

Ma, L.W., Flerchinger, G.N., Ahuja, L.R., Sauer, T.J., Prueger, J.H., Malone, R.W., Hatfield, J.L., 2012b. Simulating the surface energy balance in a soybean canopy with the SHAW and RZ-SHAW models. Trans. ASABE 55 (1), 175–179. https://doi.org/10.13031/2013.41261.

Ma, L.W., Hoogenboom, G., Ahuja, L.R., Ascough II, J.C., Saseendran, S.A., 2006. Evaluation of the RZWQM-CERES-Maize hybrid model for maize production. Agric. Syst. 87 (3), 274–295. https://doi.org/10.1016/j.agsy.2005.02.001.

Mahrer, Y., Naot, O., Rawitz, E., Katan, J., 1984. Temperature and moisture regimes in soils mulched with transparent polyethylene. Soil Sci. Soc. Am. J. 48 (2), 362–367. https://doi.org/10.2136/sssaj1984.03615995004800020028x.

Malone, R.W., Jaynes, D.B., Ma, L.W., Nolan, B.T., Meek, D.W., Karlen, D.L., 2010. Soil-test N recommendations augmented with PEST-optimized RZWQM simulations. J. Environ. Qual. 39 (5), 1711–1723. https://doi.org/10.2134/jeq2009.0425.

Ran, H., Kang, S.Z., Li, F.S., Tong, L., Ding, R.S., Du, T.S., Li, S., Zhang, X.T., 2017. Performance of AquaCrop and SIMDualKc models in evapotranspiration partitioning on full and deficit irrigated maize for seed production under plastic film-mulch in an arid region of China. Agric. Syst. 151, 20–32. https://doi.org/10.1016/j.agsy.2016.11.001.

Steinmetz, Z., Wollmann, C., Schaefer, M., Buchmann, C., David, J., Troeger, J., Munoz, K., Fror, O., Schaumann, G.E., 2016. Plastic mulching in agriculture. Trading short-term agronomic benefits for long-term soil degradation? Sci. Total Environ. 550, 690–705. https://doi.org/10.1016/j.scitotenv.2016.01.153.

Tan, S., Wang, Q.J., Zhang, J.H., Chen, Y., Shan, Y.Y., Xu, D., 2018. Performance of AquaCrop model for cotton growth simulation under film-mulched drip irrigation in southern Xinjiang, China. Agric. Water Manag. 196, 99–113. https://doi.org/10.1016/j.agwat.2017.11.001.

Thorp, K.R., Hunsaker, D.J., French, A.N., 2010. Assimilating leaf area index estimates from remote sensing into the simulations of a cropping systems model. Am. Soc. Agric. Biol. Eng. 53 (1), 251–262. https://doi.org/10.13031/2013.29490.

Wang, S.S., Deng, G.Y., 1991. A study on the mechanism of soil temperature in creasing under plastic mulch. Sci. Agric. Sin. (03), 74–78.

Wu, C.L., Chau, K.W., Huang, J.S., 2007. Modelling coupled water and heat transport in a soil-mulch-plant-atmosphere continuum (SMPAC) system. Appl. Math. Modell. 31 (2), 152–169. https://doi.org/10.1016/j.apm.2005.08.018.

Wu, Y., Huang, F.Y., Jia, Z.K., Ren, X.L., Cai, T., 2017. Response of soil water, temperature, and maize (*Zea may* L.) production to different plastic film mulching patterns in semi-arid areas of northwest China. Soil Tillage Res. 166, 113–121. https://doi.org/10.1016/j.still.2016.10.012.

Yang, Q.D., Zuo, H.C., Xiao, X., Wang, S.J., Chen, B.L., Chen, J.W., 2012. Modelling the effects of plastic mulch on water, heat and CO_2 fluxes over cropland in an arid region. J. Hydrol. 452, 102–118. https://doi.org/10.1016/j.jhydrol.2012.05.041.

Yu, Q., Flerchinger, G.N., Xu, S., Kozak, J., Ma, L.W., Ahuja, L.R., 2007. Energy balance simulation of a wheat canopy using the RZ-SHAW (RZWQM-SHAW) model. Trans. ASABE 50 (5), 1507. https://doi.org/10.13031/2013.23948.

Zhang, F., Zhang, W.J., Qi, J.G., Li, F.M., 2018a. A regional evaluation of plastic film mulching for improving crop yields on the Loess Plateau of China. Agric. For. Meteorol. 248, 458–468. https://doi.org/10.1016/j.agrformet.2017.10.030.

Zhang, Y.Q., Wang, J.D., Gong, S.H., Xe, D., Sui, J., Wu, Z.D., Mo, Y., 2018b. Effects of film mulching on evapotranspiration, yield and water use efficiency of a maize field with drip irrigation in Northeastern China. Agric. Water Manag. 205, 90–99. https://doi.org/10.1016/j.agwat.2018.04.029.